

# Mound formation and coarsening from a nonlinear instability in surface growth

Buddhapriya Chakrabarti and Chandan Dasgupta\*

Centre for Condensed Matter Theory, Department of Physics, Indian Institute of Science, Bangalore 560012, INDIA  
and

Condensed Matter Theory Unit, JNCASR, Bangalore 560064, INDIA

(November 21, 2018)

We study a class of one-dimensional, nonequilibrium, conserved growth equations for both non-conserved and conserved noise statistics using numerical integration. An atomistic version of these growth equations is also studied using stochastic simulation. The models with nonconserved noise statistics are found to exhibit mound formation and power-law coarsening with slope selection for a range of values of the model parameters. Unlike previously proposed models of mound formation, the Ehrlich-Schwoebel step-edge barrier, usually modeled as a linear instability in growth equations, is absent in our models. Mound formation in our models occurs due to a nonlinear instability in which the height (depth) of spontaneously generated pillars (grooves) increases rapidly if the initial height (depth) is sufficiently large. When this instability is controlled by the introduction of an infinite number of higher-order gradient nonlinearities, the system exhibits a first-order dynamical phase transition from a rough self-affine phase to a mounded one as the value of the parameter that measures the effectiveness of control is decreased. We define a new “order parameter” that may be used to distinguish between these two phases. In the mounded phase, the system exhibits power-law coarsening of the mounds in which a selected slope is retained at all times. The coarsening exponents for the continuum equation and the discrete model are found to be different. An explanation of this difference is proposed and verified by simulations. In the growth equation with conserved noise, we find the curious result that the kinetically rough and mounded phases are both locally stable in a region of parameter space. In this region, the initial configuration of the system determines its steady-state behavior.

PACS numbers: 05.70.Ln, 64.60.Ht, 81.10.Aj, 81.15.Hi

## I. INTRODUCTION

The process of growing films by the deposition of atoms on a substrate is of considerable experimental and theoretical interest [1]. While there has been a lot of research on the process of kinetic roughening [1–3] leading to a self-affine interface profile, there has been much recent experimental [4–12] and theoretical [4,6,13–25] interest in a different mode of surface growth involving the formation of “mounds” which are pyramid-like or “wedding-cake-like” structures. The precise experimental conditions that determine whether the growth morphology would be kinetically rough or dominated by mounds are presently unclear. However, many experiments show the formation of mounds that *coarsen* (the typical lateral size of the mounds increases) with time. During this process, the typical slope of the sides of the pyramid-like mounds may or may not remain constant. If the slope remains constant in time, the system is said to exhibit *slope selection*. As the mounds coarsen, the surface roughness characterized by the root-mean-square width of the interface increases. Eventually, at very long times, the system is expected to evolve to a single-mound structure in which the mound size is equal to the system size.

There are obvious differences between the structures of kinetically rough and mounded interfaces. In the first case, the interface is rough in a self-affine way at length scales shorter than a characteristic length  $\xi(t)$  that ini-

tially increases with time and eventually saturates at a value comparable to the sample size. In the second case, the characteristic length is the typical mound size  $R(t)$  whose time-dependence is qualitatively similar to that of  $\xi(t)$ . However, the interface in this case looks well-ordered at length scales shorter than  $R(t)$ . Nevertheless, there are certain similarities between the gross features of these two kinds of surface growth. First consider the simpler situation in which the slope of the sides of the mounds remains constant in time. Simple geometry tells us that if the system evolves to a single-mound structure at long times, then the “roughness exponent”  $\alpha$  must be equal to unity. Also, the height-difference correlation function  $g(r)$  is expected to be proportional to  $r$  for  $r \ll R(t)$ . This is consistent with  $\alpha = 1$ . If the mound size  $R(t)$  increases with time as a power law,  $R(t) \sim t^n$ , during coarsening, then the interface width  $W$ , which is essentially the height of a typical mound, should also increase with time as a power law with the same exponent  $n$ . Thus, dynamic scaling with “growth exponent”  $\beta$  equal to  $n$ , and “dynamical exponent”  $z$  equal  $1/n$  is recovered. If the mound slope  $s(t)$  increases with time as a power law,  $s(t) \sim t^\theta$  (this is known in the literature as *steepening*), then one obtains behavior similar to anomalous dynamical scaling [26] with  $\beta = n + \theta$ ,  $z = 1/n$ .

These similarities between the gross scaling properties of kinetic roughening with a large value of  $\alpha$  and mound formation with power-law coarsening make it difficult to

experimentally distinguish between these two modes of surface growth. This poses a problem in the interpretation of experimental results [11,12]. Existing experiments on mound formation show a wide variety of behavior. Without going into the details of individual experiments, we note that some experiments show mound coarsening with a time-independent “magic” slope, whereas other experiments do not show any slope selection. The detailed morphology of the mounds varies substantially from one experiment to another. The reported values of the coarsening exponent  $n$  show a large variation in the range 0.15-0.4.

Traditionally, the formation of mounds has been attributed to the presence of the so-called Ehrlich-Schwoebel (ES) step-edge barrier [27,28] that hinders the downward motion of atoms across the edge of a step. This step-edge diffusion bias makes it more likely for an atom diffusing on a terrace to attach to an ascending step than to a descending one. This leads to an effective “uphill” surface current [29] that has a destabilizing effect, leading to the formation of mounded structures as the atoms on upper terraces are prevented by the ES barrier from coming down.

This destabilizing effect is usually represented in continuum growth equations by a *linear instability*. Such growth equations usually have a “conserved” form in which the time-derivative of the height is assumed to be equal to the negative of the divergence of a nonequilibrium surface current  $\mathbf{j}$ . The effects of an ES barrier are modeled in these equations by a term in  $\mathbf{j}$  that is proportional to the gradient of the height (for small values of the gradient) with a *positive* proportionality constant. Such a term is manifestly unstable, leading to unlimited exponential growth of the  $\mathbf{k} \neq 0$  Fourier components of the height. This instability has to be controlled by other nonlinear terms in the growth equation in order to obtain a proper description of the long-time behavior. A number of different choices for the nonlinear terms have been reported in the literature [4,6,13,14,22,23]. If the “ES part” of  $\mathbf{j}$  has one or more stable zeros as a function of the slope  $\mathbf{s}$ , then the slope of the mounds that form as a result of the ES instability is expected to stabilize at the corresponding value(s) of  $\mathbf{s}$  at long times. The system would then exhibit slope selection. If, on the other hand, this part of  $\mathbf{j}$  does not have a stable zero, then the mounds are expected to continue to steepen with time. Analytic and numerical studies of such continuum growth equations have produced a wide variety of results, such as power-law coarsening and slope selection with  $n = 1/4$  [13] or  $n \simeq 0.17$  [6] in two dimensions, power-law coarsening accompanied by a steepening of the mounds [4,14,16], and a complex coarsening process [22,23] in which the growth of the mound size becomes extremely slow after a characteristic size is reached.

There are several atomistic, cellular-automaton-type models [19–21] that incorporate the effects of an ES diffusion barrier. Formation and coarsening of mounds in the presence of an ES barrier have also been studied [22,23]

in a 1d model with both discrete and continuum features. We also note that a new mechanism for mounding instability has been discovered recently [17,18]. This instability, generated by fast diffusion along the edges of monatomic steps, leads to the formation of quasi-regular shaped mounds in two or higher dimensions. The effects of this instability have been studied in simulations [17,18,20,24,25]. The wide variety of results [17–25] obtained from simulations of different models, combined with similar variations in the experimental results, have made it very difficult to identify the microscopic mechanism of mound formation in surface growth.

In this paper, we show that mound formation, slope selection and power-law coarsening in a class of one-dimensional (1d) continuum growth equations and discrete atomistic models can occur from a mechanism that is radically different from the ones mentioned above. Our study is based on the conserved nonlinear growth equation proposed by Villain [29] and by Lai and Das Sarma [30], and an atomistic version [31] of this equation. We have studied the behavior of the continuum equation by numerical integration, and the behavior of the atomistic model by stochastic simulation. Previous work [32–34] on these systems showed that they exhibit a *nonlinear* instability, in which pillars (grooves) with height (depth) greater than a critical value continue to grow rapidly. This instability can be controlled [32–34] by the introduction of an infinite number of higher-order gradient nonlinearities. When the parameter that describes the effectiveness of control is sufficiently large, the controlled models exhibit [32–34] kinetic roughening, characterized by usual dynamical scaling with exponent values close to those expected from dynamical renormalization group calculations [30]. As the value of the control parameter is decreased, these models exhibit transient multiscaling [32–34] of height fluctuations. For yet smaller values of the control parameter, the rapid growth of pillars or grooves causes a breakdown of dynamical scaling, with the width versus time plot showing a sharp upward deviation [33] from the power-law behavior found at short times (before the onset of the nonlinear instability).

We report here the results of a detailed study of the behavior of these models in the regime of small values of the control parameter where conventional kinetic roughening is not observed. We find that in this regime, the interface self-organizes into a sawtooth-like structure with a series of triangular, pyramid-like mounds. These mounds coarsen in time, with larger mounds growing at the expense of smaller ones. In this coarsening regime, a power-law dependence of the interface width on time is recovered. The slope of the mounds remains constant during the coarsening process. In section II, the growth equation and the atomistic model studied in this work are defined and the numerical methods we have used to analyze their behavior are described. The basic phenomenology of mound formation and slope selection in these systems is described in detail in section III. Specifically, we

show that the nonlinear mechanism of mound formation in these systems is “generic” in the sense that the qualitative behavior does not depend on the specific form of the function used for controlling the instability. In particular, we find very similar behavior for two different forms of the control function: one used in earlier studies [32–34] of these systems, and the other one proposed by Politi and Villain [23] from physical considerations. Since the linear instability used conventionally to model the ES mechanism is explicitly absent in our models, our work shows that the presence of step-edge barriers is not essential for mound formation. The slope selection found in our models is a true example of nonlinear pattern formation: since the nonequilibrium surface current in our models vanishes for all values of constant slope, the selected value of the slope can not be predicted in any simple way. This is in contrast to the behavior of ES-type models where slope selection occurs only if the surface current vanishes at a specific value of the slope.

Next, in section IV, we show that the change in the dynamical behavior of the system (from kinetic roughening to mound formation and coarsening) may be described as a first-order nonequilibrium phase transition. Since the instability in our models is a nonlinear one, the flat interface is locally stable in the absence of noise for all values of the model parameters (the strength of the nonlinearity and the value of the control parameter). The mounded phase corresponds to a different stationary solution of the dynamical equations in the absence of noise. We use a linear stability analysis to find the “spinal boundary” in the two-dimensional parameter space across which the mounded stationary solution becomes locally unstable. We show that the results of this numerical stability analysis can also be obtained from simple analytic arguments. To obtain the phase boundary in the presence of noise, we first define an *order parameter* that is zero in the kinetically rough phase and nonzero in the mounded phase. We combine the numerically obtained results for this order parameter for different sample sizes with finite-size scaling to confirm that this order parameter exhibits the expected behavior in the two phases. The phase boundary that separates the mounded phase from the kinetically rough one is obtained numerically. The phase boundaries for the continuum model with two different forms of the control function and the atomistic model are found to be qualitatively similar.

The results of a detailed study of the process of coarsening of the mounds are reported in section V. Surprisingly, we find that the coarsening exponents of the continuum equation and its atomistic version are different. We propose a possible explanation of this result on the basis of an analysis of the coarsening process in which the problem is mapped to that of a Brownian walker in an attractive force field. In this mapping, the Brownian walk is supposed to describe the noise-induced random motion of the peak of a mound, and the attractive “force” represents the interaction between neighboring mounds that leads to coarsening. We show that the numerical results

obtained for the dynamics of mounds in the atomistic model are consistent with this explanation.

In section VI, we consider the behavior of the continuum growth equation for “conserved” noise statistics. The nonlinear instability found in the nonconserved case is expected to be present in the conserved case also. However, there is an important difference between the two cases. The nonconserved model exhibits anomalous dynamical scaling, so that the typical nearest-neighbor height difference continues to increase with time, and the instability is always reached [33] at sufficiently long times, even if the starting configuration is perfectly flat. Since the continuum model with conserved noise statistics exhibits [35] usual dynamic scaling with  $\alpha < 1$ , the nearest-neighbor height difference is expected to saturate at long times if the initial state of the system is flat. Under these circumstances, the occurrence of the nonlinear instability in runs started from flat states would depend on the values of the parameters. Specifically, the instability may not occur at all if the value of the nonlinear coefficient in the growth equation is sufficiently small. At the same time, the instability can be initiated by choosing an initial state with sufficiently high (deep) pillars (grooves). Since mound formation in these models is crucially dependent on the occurrence of the instability, the arguments above suggest that the nature of the long-time steady state reached in the conserved model may depend on the choice of the initial state. Indeed, we find from simulations that in a region of parameter space, the mounded and kinetically rough phases are both locally stable and the steady state configuration is determined by the choice of the initial configuration of the interface. These results imply the surprising conclusion that the long-time, steady-state morphology of a growing interface, as well as the dynamics of the process by which the steady state is reached may be “history dependent” in the sense that the behavior would depend crucially on the choice of the initial state. A summary of our findings and a discussion of the implications of our results are provided in Sec.VII. A summary of the basic results of our study was reported in a recent Letter [36].

## II. MODELS AND METHODS

Conserved growth equations (deterministic part of the dynamics having zero time derivative for the  $\mathbf{k} = 0$  Fourier mode of the height variable) with nonconserved noise are generally used [2] to model nonequilibrium surface growth in molecular beam epitaxy (MBE). The conservation is a consequence of absence of bulk vacancies, overhangs and desorption (evaporation of atoms from the substrate) under optimum MBE growth conditions. Thus, integrating over the whole sample area gives the number of particles deposited. This conservation is not strictly valid because of “shot noise” fluctuations in the beam. The shot noise is modeled by an additive noise

term  $\eta(\mathbf{r}, t)$  in the equation of motion of the interface. The noise  $\eta$  is generally assumed to be delta-correlated in both space and time:

$$\langle \eta(\mathbf{r}, t) \eta(\mathbf{r}', t') \rangle = 2D \delta^d(\mathbf{r} - \mathbf{r}') \delta(t - t'), \quad (1)$$

where  $\mathbf{r}$  is a point on a  $d$ -dimensional substrate. Thus, a conserved growth equation may be written in a form

$$\frac{\partial h}{\partial t} = -\nabla \cdot \mathbf{j} + \eta, \quad (2)$$

where  $h(\mathbf{r}, t)$  is the height at point  $\mathbf{r}$  at time  $t$ , and  $\mathbf{j}$  is the surface current density. The surface current models the deterministic dynamics at the growth front. As mentioned in section I, the presence of an ES step-edge barrier is modeled in continuum equations of the form of Eq.(2) by a term in  $\mathbf{j}$  that is proportional to the slope  $\mathbf{s} = \nabla h$ , with a positive constant of proportionality. This makes the flat surface ( $h(\mathbf{r})$  constant for all  $\mathbf{r}$ ) linearly unstable. This instability is controlled by the introduction of terms involving higher powers of the local slope  $\mathbf{s}$  and higher-order spatial derivatives of  $h$ .

We consider the conserved growth equation proposed by Villain [29] and Lai and Das Sarma [30] for describing MBE-type surface growth *in the absence of ES step-edge barriers*. This equation is of the form

$$\partial h'(\mathbf{r}, t') / \partial t' = -\nu \nabla^4 h' + \lambda' \nabla^2 |\nabla h'|^2 + \eta'(\mathbf{r}, t'), \quad (3)$$

where  $h'(\mathbf{r}, t')$  represents the height variable at the point  $\mathbf{r}$  at time  $t'$ . This equation is believed [2] to provide a correct description of the kinetic roughening behavior observed in MBE-type experiments [12].

In our study, we numerically integrate the 1d version of Eq.(3) using a simple Euler scheme [33]. Upon choosing appropriate units of length and time and discretizing in space and time, Eq.(3) is written as [33]

$$h_i(t + \Delta t) - h_i(t) = \Delta t \tilde{\nabla}^2 [-\tilde{\nabla}^2 h_i(t) + \lambda |\tilde{\nabla} h_i(t)|^2] + \sqrt{\Delta t} \eta_i(t), \quad (4)$$

where  $h_i(t)$  represents the dimensionless height variable at the lattice point  $i$  at dimensionless time  $t$ ,  $\tilde{\nabla}$  and  $\tilde{\nabla}^2$  are lattice versions of the derivative and Laplacian operators, and  $\eta_i(t)$  is a random variable with zero average and variance equal to unity. These equations, with an appropriate choice of  $\Delta t$ , are used to numerically follow the time evolution of the interface. In most of our studies, we have used the following definitions for the lattice derivatives:

$$\begin{aligned} \tilde{\nabla} h_i &= (h_{i+1} - h_{i-1})/2, \\ \tilde{\nabla}^2 h_i &= h_{i+1} + h_{i-1} - 2h_i. \end{aligned} \quad (5)$$

We have checked that the use of more accurate, left-right symmetric definitions of the lattice derivatives, involving more neighbors to the left and to the right [33], leads to

results that are very similar to those obtained from calculations in which these simple definitions are used. We have also checked that the results obtained in the deterministic limit ( $\eta = 0$ ) by using a more sophisticated integration routine [37] closely match those obtained from the Euler method with sufficiently small values of the integration time step.

We have also studied an atomistic version [31] of Eq.(3) in which the height variables  $\{h_i\}$  are integers. This model is defined by the following deposition rule. First, a site (say  $i$ ) is chosen at random. Then the quantity

$$K_i(\{h_j\}) = -\tilde{\nabla}^2 h_i + \lambda |\tilde{\nabla} h_i|^2 \quad (6)$$

is calculated for the site  $i$  and all its nearest neighbors. Then, a particle is added to the site that has the smallest value of  $K$  among the site  $i$  and its nearest neighbors. In the case of a tie for the smallest value, the site  $i$  is chosen if it is involved in the tie; otherwise, one of the sites involved in the tie is chosen randomly. The number of deposited layers provides a measure of time in this model.

It was found in earlier studies [32–34] that both these models exhibit a *nonlinear instability* in which isolated structures (pillars for  $\lambda > 0$ , grooves for  $\lambda < 0$ ) grow rapidly if their height (depth) exceeds a critical value. This instability can be controlled [32–34] by replacing  $|\tilde{\nabla} h_i|^2$  in Eqns.(4) and (6) by  $f(|\tilde{\nabla} h_i|^2)$  where the nonlinear function  $f(x)$  is defined as

$$f(x) = \frac{1 - e^{-cx}}{c}, \quad (7)$$

$c > 0$  being a control parameter. We call the resulting models “model I” and “model II”, respectively. This replacement, amounts to the introduction of an infinite series of higher-order nonlinear terms. The time evolution of the height variables in model I is, thus, given by

$$h_i(t + \Delta t) - h_i(t) = \Delta t \tilde{\nabla}^2 [-\tilde{\nabla}^2 h_i(t) + \lambda (1 - e^{-c|\tilde{\nabla} h_i(t)|^2})/c] + \sqrt{\Delta t} \eta_i(t). \quad (8)$$

In model II, the quantity  $K_i$  is defined as

$$K_i(\{h_j\}) = -\tilde{\nabla}^2 h_i + \lambda (1 - e^{-c|\tilde{\nabla} h_i|^2})/c. \quad (9)$$

While the function  $f(x)$  was introduced in the earlier work purely for the purpose of controlling the nonlinear instability, it turns out that the introduction of this function in the growth equation is physically meaningful. Politi and Villain [23] have shown that the nonequilibrium surface current that leads to the  $\nabla^2 |\nabla h'|^2$  term in Eq.(3) should be proportional to  $\nabla |\nabla h'|^2$  when  $|\nabla h'|$  is small, and should go to zero when  $|\nabla h'|$  is large. The introduction of the “control function”  $f(|\tilde{\nabla} h_i|^2)$  satisfies this physical requirement. We have also carried out studies of a slightly different model (which we call “model IA”) in which the function  $f(x)$  is assumed to have a form suggested by Politi and Villain:

$$f(x) = \frac{x}{1+cx}, \quad (10)$$

where  $c$  is, as before, a positive control parameter. This function has the same asymptotic behavior as that of the function defined in Eq.(7). As we shall show later, the results obtained from calculations in which these two different forms of  $f(x)$  are used are qualitatively very similar. In fact, we expect that the qualitative behavior of these models would be the same for any monotonic function  $f(x)$  that satisfies the following requirements: (i)  $f(x)$  must be proportional to  $x$  in the small- $x$  limit; and (ii) it must saturate to a constant value as  $x \rightarrow \infty$ .

We have carried out extensive simulations of both these models for different system sizes. The results reported here have been obtained for systems of sizes  $40 \leq L \leq 1000$ . There is no significant dependence of the results on  $L$ . The time step used in most of our studies of models I and IA is  $\Delta t = 0.01$ . We have checked that very similar results are obtained for smaller values of  $\Delta t$ . We used both unbounded (Gaussian) and bounded distributions for the random variables  $\eta_i$  in our simulations of models I and IA, with no significant difference in the results. For computational convenience, a bounded distribution (uniform between  $+\sqrt{3}$  and  $-\sqrt{3}$ ) was used in most of our calculations. Unless otherwise stated, the results described in the following sections were obtained using periodic boundary conditions. The effects of using other boundary conditions will be discussed in the next section.

### III. MOUND FORMATION AND SLOPE SELECTION

It has been demonstrated earlier [32,33] that if the control parameter  $c$  is sufficiently large, then the nonlinear instability is completely suppressed and the models exhibit the usual dynamical scaling behavior with the expected [30] exponent values,  $\beta \simeq 1/3$ ,  $z \simeq 3$ , and  $\alpha = \beta z \simeq 1$ . This behavior for model I is illustrated by the solid line in Fig.1, which shows a plot of the width  $W$  as a function of time  $t$  for parameter values  $\lambda=4.0$  and  $c = 0.06$ . As the value of  $c$  is decreased with  $\lambda$  held constant, the instability makes its appearance: the height  $h_0$  of an isolated pillar (for  $\lambda > 0$ ) increases in time if  $h_{min}(\lambda, c) < h_0 < h_{max}(\lambda, c)$ . The value of  $h_{min}$  is nearly independent of  $c$ , while  $h_{max}$  increases as  $c$  is decreased [33]. If  $c$  is sufficiently large,  $h_{max}$  is small and the instability does not affect the scaling behavior of global quantities such as  $W$ , although transient multiscaling at length scales shorter than the correlation length  $\xi \sim t^{1/z}$  may be found [32,33] if  $c$  is not very large. As  $c$  is decreased further,  $h_{max}$  becomes large, and when isolated pillars with  $h_0 > h_{min}$  are created at an initially flat interface through fluctuations, the rapid growth of such pillars to height  $h_{max}$  leads to a sharp upward departure from the power-law scaling of  $W$  with

time  $t$ . The time at which this departure occurs varies from run to run. This behavior for model I with  $\lambda = 4.0$  and  $c = 0.02$  is shown by the dash-dotted line in Fig.1.

This instability leads to the formation of a large number of randomly distributed pillars of height close to  $h_{max}$ . As the system evolves in time, the interface self-organizes to form triangular mounds of a fixed slope near these pillars. These mounds then coarsen in time, with large mounds growing larger at the expense of small ones. In this coarsening regime, a power-law growth of  $W$  in time is recovered. The slope of the sides of the triangular mounds remains constant during this process. Finally, the system reaches a steady state with one peak and one trough (if periodic boundary conditions are used) and remains in this state for longer times. The interface profiles in the kinetically rough phase (obtained for relatively large values of  $c$ ) and the mounded phase (obtained for small  $c$ ) are qualitatively different. This difference is illustrated in Fig.2 that shows typical interface profiles in the two different phases. This figure also shows a typical interface profile for model IA in the mounded regime, illustrating the fact that the precise choice of the control function  $f(x)$  is not crucial for the formation of mounds. The evolution of the interface structure in the mounded regime of model I is illustrated in Fig.3 which shows the interface profiles obtained in a typical  $L = 200$  run starting from a flat initial state at three different times:  $t = 200$  (before the onset of the instability),  $t = 4000$  (after the onset of the instability, in the coarsening regime), and  $t = 128000$  (in the final steady state). This figure also shows the steady-state interface profile of a  $L = 500$  sample with the same parameters, to illustrate that the results do not depend on the sample size.

Very similar behavior is found for model II. Since the heights in this atomistic model can increase only by discrete amounts in each unit of discrete time, the increase of  $W$  at the onset of the instability is less rapid here than in the continuum models I and IA. Nevertheless, the occurrence of the instability for small values of  $c$  shows up as a sharp upward deviation of the  $W$  versus  $t$  plot from the initial power-law behavior with  $\beta \simeq 1/3$ . This is illustrated by the dash-dotted line in Fig.4, obtained from simulations of model II with  $\lambda = 2.0$ ,  $c = 0.005$ . This behavior is to be contrasted with that for  $\lambda = 2.0$ ,  $c = 0.015$ , shown by the full line in Fig.4, where the nonlinear instability is absent. The difference between the surface morphologies in the two regimes of model II is illustrated in Fig.5. The kinetically rough, self-affine morphology obtained for  $c = 0.02$  is clearly different from the mounded profile found for  $c = 0.005$ . The time evolution of the interface in the mounded regime of this model is illustrated in Fig.6. The general behavior is clearly similar to that found for models I and IA. This figure also shows a properly scaled plot of the interface profile of a  $L = 500$  sample with the same parameters at a time in the coarsening regime. It is clear from this plot that the nature of the interface and the value of the selected slope do not depend on the sample size.

The occurrence of a peak and a symmetrically placed trough in the steady-state profiles shown in Figs 3 and 6 is a consequence of using periodic boundary conditions. The deterministic part of the growth equation of Eq.(8) strictly conserves the average height if periodic boundary conditions are used. So, the average height remains very close to zero if the initial state is flat, as in most of our simulations. The steady-state profile must have at least one peak and one trough in order to satisfy this requirement. Also, it is easy to show that if the slopes of the "uphill" and "downhill" parts of the steady-state profile are the same in magnitude (this is true for our models), then the two extrema must be separated by  $\simeq L/2$ . Therefore, it is clear that the steady state obtained in simulations with periodic boundary conditions must have a peak and a symmetrically placed trough separated by distance  $\simeq L/2$ .

To check whether the basic phenomenology described above depends on the choice of the boundary condition, we have carried out test simulations using two other boundary conditions: "fixed" boundary condition, in which the height variable to the left of  $i = 1$ , and to the right of  $i = L$  are pinned to zero at all times; and "zero flux" boundary condition with vanishing first and third derivatives of the height at the two ends of the sample. For these boundary conditions, the deterministic part of the growth equation does not strictly conserve the average height. As a result, the symmetry between the mound and the trough, found in the long-time steady state obtained for periodic boundary condition, is not present if one of the other boundary conditions is used. In particular, it is possible to stabilize a single mound or a single trough in the steady state for the other boundary conditions. Since the heights at the two ends must be the same for fixed boundary condition, the two extrema in a configuration with one mound and one trough must be separated by  $\simeq L/2$ , as shown in Fig.7. The two extrema would not be separated by  $\simeq L/2$  for the zero-flux boundary condition. These effects of boundary conditions are illustrated in Fig.7 which shows profiles in the mounded regime obtained for the three different boundary conditions mentioned above. It is clear from the results shown in this figure that the basic phenomenology, i.e. the formation and coarsening of mounds and slope selection, is not affected by the choice of boundary conditions. In particular, the values of the selected slope and the heights of the pillars at the top of a mound and the bottom of a trough remain unchanged when boundary conditions other than periodic are used.

The selection of a "magic slope" during the coarsening process is clearly seen in the plots of Fig.3 and Fig.6. More quantitatively, the probability distribution of the magnitude of the nearest-neighbor height differences  $s_i \equiv |h_{i+1} - h_i|$  is found to exhibit a pronounced peak at the selected value of the slope, and the position of this peak does not change during the coarsening process. Fig.8 shows a comparison of the distribution of the magnitude of the nearest-neighbor height difference for

model I in the mounded and kinetically rough phases. A bimodal distribution is seen for the mounded phase, the two peaks corresponding to the values of the selected slope and the height of the pillars at the top and bottom of the pyramids. The kinetically rough phase, on the other hand, exhibits a distribution peaked at zero. Fig.9 shows the values of the selected slope at different times in the coarsening regime of model I. The constancy of the slope is clearly seen in this plot. All these features remain true for the discrete model. Plots of the distribution  $P(s)$  at two different times in the coarsening regime of model II are shown in Fig.10. The peak position shows a small shift in the positive direction as  $t$  is increased, but this shift is small compared to the width of the distributions, indicating near constancy of the selected slope. The value of the selected slope depends on the parameters  $\lambda$  and  $c$ . This is discussed in the next section.

#### IV. DYNAMICAL PHASE TRANSITION

The instability that leads to mound formation in our models is a nonlinear one, so that the perfectly flat state of the interface is a locally stable steady-state solution of the zero-noise growth equation for all parameter values. When the instability is absent (e.g. for large values of the control parameter  $c$ ), this "fixed-point" solution of the noise-free equation is transformed to the kinetically rough steady state in the presence of noise. The mounded steady state obtained for small values of  $c$  must correspond to a different fixed point of the zero-noise growth equation. Such nontrivial fixed-point solutions may be obtained from the following simple calculation.

The profile near the top ( $i = i_0$ ) of a triangular mound may be approximated as  $h_{i_0} = x_0 + x_1$ ,  $h_{i_0+j} = x_0 - (|j| - 1)x_2$ , where  $x_1$  is the height of the pillar at the top of the mound and  $x_2$  is the selected slope. This profile would not change under the dynamics of Eq.(8) with no noise if the following conditions are satisfied:

$$\begin{aligned} & \tilde{\nabla}^2 h_{i_0} - \lambda(1 - e^{-c|\tilde{\nabla} h_{i_0}|^2})/c \\ &= \tilde{\nabla}^2 h_{i_0 \pm 1} - \lambda(1 - e^{-c|\tilde{\nabla} h_{i_0 \pm 1}|^2})/c \\ &= \tilde{\nabla}^2 h_{i_0 \pm 2} - \lambda(1 - e^{-c|\tilde{\nabla} h_{i_0 \pm 2}|^2})/c. \end{aligned} \quad (11)$$

These conditions lead to the following pair of non-linear equations for the variables  $x_1$  and  $x_2$  used to parametrize the profile near the top of a mound:

$$\begin{aligned} 2x_1 - \lambda[1 - e^{-cx_2^2}]/c &= 0, \\ 3x_1 - x_2 - \lambda[1 - e^{-c(x_1+x_2)^2/4}]/c &= 0. \end{aligned} \quad (12)$$

These equations admit a non-trivial solution for sufficiently small  $c$ , and the resulting values of  $x_1$  and  $x_2$  are found to be quite close to the results obtained from numerical integration. A similar analysis for the profile near the bottom of a trough (this amounts to replacing  $x_2$  by  $-x_2$  in Eq.(12)) yields slightly different values for  $x_1$  and

$x_2$ . The full stable profile (a fixed point of the dynamics without noise) with one peak and one trough may be obtained numerically by calculating the values of  $\{h_i\}$  for which  $g_i$ , the term multiplying  $\Delta t$  in the right-hand side of Eq.(8), is zero for all  $i$ . The fixed-point values of  $\{h_i\}$  satisfy the following equations:

$$g_i = \tilde{\nabla}^2[-\tilde{\nabla}^2 h_i + \lambda(1 - e^{-c|\tilde{\nabla} h_i|^2})/c] = 0 \text{ for all } i. \quad (13)$$

A numerical solution of these coupled nonlinear equations shows that the small mismatch between the values of  $x_2$  near the top and the bottom is accommodated by creating a few ripples near the top. The numerically obtained fixed-point profile for a  $L = 500$  system with  $\lambda = 4.0$ ,  $c = 0.02$  is shown in Fig.11, along with a typical steady-state profile for the same system. The two profiles are found to be nearly identical, indicating that the mounded steady state in the presence of noise corresponds to this fixed-point solution of the noiseless discretized growth equation.

Fixed-point solutions of the continuum equation, Eq.(3), with  $\nu = 1$  and  $|\nabla h|^2$  replaced by  $f(|\nabla h|^2)$  where  $f(x)$  has the form shown in Eq.(10) may also be obtained by a semi-analytical approach following Racz *et al.* [38]. We consider stationary solutions of the continuum equation that satisfy the following first-order differential equation with appropriate boundary conditions:

$$-\frac{ds}{dx} + \lambda \frac{s^2}{1 + cs^2} = A, \quad (14)$$

where  $s(x) = dh(x)/dx$  is the local slope of the interface and  $A$  is a constant that must be positive in order to obtain a solution that resembles a triangular mound. At large distances from the peak of the mound, the slope  $s$  would be constant, so that  $ds(x)/dx$  would vanish, whereas the second term would give a positive contribution if  $\lambda$  is positive. At the peak of the profile, the second term would be zero because  $s$  is zero, but  $ds(x)/dx$  would be negative, making the left-hand side of Eq.(14) positive. While a closed-form solution of this differential equation cannot be obtained, the value of  $s(x)$  at any point  $x$  may be calculated with any desired degree of accuracy by numerically solving a simple algebraic equation. The height profile is then obtained by integrating  $s(x)$  with appropriate boundary conditions. In our calculation, we used the procedure of Racz *et al.* [38] to take into account periodic boundary conditions. In Fig. 11, we have shown a typical steady-state profile of a  $L = 200$  sample of model IA with  $\lambda = 4.0$  and  $c = 0.01$ , and a fixed-point solution of the corresponding continuum equation. The value of the constant  $A$  in Eq.(14) was chosen to yield the same slope as that of the steady-state profile of the discrete model. These results show that the steady-state properties for the two forms of  $f(x)$  are very similar, and the continuum equation admits stationary solutions that are very similar to those of the discretized models.

The local stability of the mounded fixed point may be determined from a calculation of the eigenvalues of the stability matrix,  $M_{ij} = \partial g_i / \partial h_j$ , evaluated at the fixed point. We find that the largest eigenvalue of this matrix (disregarding the trivial zero eigenvalue associated with an uniform displacement of the interface,  $h_i \rightarrow h_i + \delta$  for all  $i$ ) crosses zero at  $c = c_1(\lambda)$  (see Fig.(12)), signaling an instability of the mounded profile. The structure of Eq.(8) implies that  $c_1(\lambda) \propto \lambda^2$ . Thus, for  $0 < c < c_1(\lambda)$ , the dynamics of Eq.(8) without noise admits two locally stable invariant profiles: a trivial, flat profile with  $h_i$  the same for all  $i$ , and a non-trivial one with one mound and one trough. Depending on the initial state, the noiseless dynamics takes the system to one of these two fixed points. For example, an initial state with one pillar on a flat background is driven by the noiseless dynamics to the flat fixed point if the height of the pillar is smaller than a critical value, and to the mounded one otherwise.

The ‘‘relevant’’ perturbation that makes the mounded fixed point unstable at  $c = c_1$  is a uniform vertical relative displacement of the segment of the interface between the peak and the trough of the fixed-point profile. This can be seen by numerically evaluating the right eigenvector corresponding to the eigenvalue of the stability matrix that crosses zero at  $c = c_1$ . This is demonstrated in the inset of Fig.12. Also, examination of the time evolution of the mounded structure for values of  $c$  slightly higher than  $c_1$  shows that the instability of the structure first appears at the bottom of the trough. Taking cue from these observations, the value  $c_1$  can be obtained from a simple calculation. We consider the profile near the bottom of a trough at  $i = i_0$ . As discussed above, the profile near  $i_0$  may be parametrized as  $h_{i_0} = x_0 + x_1$ ,  $h_{i_0+j} = x_0 + (|j| - 1)x_2$ , and the values of  $x_1$  and  $x_2$  may be obtained by solving a pair of nonlinear equations, Eq.(12) with  $x_2$  replaced by  $-x_2$ . We now consider a perturbation of this profile, in which the heights on one side of  $i_0$  are all increased by a small amount  $\delta$  (i.e.  $h_{i_0+j} = x_0 + (j - 1)x_2 + \delta$ ,  $h_{i_0-j} = x_0 + (j - 1)x_2$  with  $j > 0$ ), and use Eq.(8) to calculate how  $\delta$  changes with time, assuming its value to be small. The requirement that  $\delta$  must decrease with time for the fixed-point structure to be locally stable leads to the following equation for the value of  $c$  at which the structure becomes unstable:

$$\frac{\lambda}{2}(x_1 - x_2)e^{-c(x_1 - x_2)^2/4} = 1, \quad (15)$$

By substituting the numerically obtained values of  $x_1$  and  $x_2$  in this equation, the critical value,  $c_1(\lambda)$ , of the parameter  $c$  is obtained as a function of  $\lambda$ . The values obtained this way are in good agreement with those obtained from our full numerical calculation of the eigenvalues of the stability matrix. The ‘‘spinodal’’ lines (i.e. the lines in the  $c - \lambda$  plane beyond which the mounded fixed point is unstable) for models I and IA are shown in Fig.13. Both these lines have the expected form,  $c_1(\lambda) \propto \lambda^2$ . It would be interesting to carry out a similar stability anal-

ysis for the mounded stationary profile (see Fig.11) of the continuum equation corresponding to model IA. Such a calculation would have to be performed *without discretizing space* if we want to address the question of whether the behavior of the truly continuum equation is similar to that of the discretized versions considered here. We have not succeeded in carrying out such a calculation: since the mounded stationary profiles for the continuum equation are obtained from a numerical calculation, it would be extremely difficult, if not impossible, to carry out a linear stability analysis for such stationary solutions without discretizing space.

In the presence of the noise, the perfectly flat fixed point transforms to the kinetically rough steady state, and the non-trivial fixed point evolves to the mounded steady state shown in Fig.11. A dynamical phase transition at  $c = c_2(\lambda) < c_1(\lambda)$  separates these two kinds of steady states. To calculate  $c_2(\lambda)$ , we start a system at the mounded fixed point and follow its evolution according to Eq.(8) for a long time (typically  $t = 10^4$ ) to check whether it reaches a kinetically rough steady state. By repeating this procedure many times, the probability,  $P_1(\lambda, c)$ , of a transition to a kinetically rough state is obtained. For fixed  $\lambda$ ,  $P_1$  increases rapidly from 0 to 1 as  $c$  is increased above a critical value. Typical results for  $P_1$  as a function of  $c$  for model I with  $\lambda = 4.0$  are shown in the inset of Fig.13. The value of  $c$  at which  $P_1 = 0.5$  provides an estimate of  $c_2$ . Another estimate is obtained from a similar calculation of  $P_2(\lambda, c)$ , the probability that a flat initial state evolves to a mounded steady state. As expected,  $P_2$  increases sharply from 0 to 1 as  $c$  is decreased (see inset of Fig.13), and the value of  $c$  at which this probability is 0.5 is slightly lower than the value at which  $P_1 = 0.5$ . This difference reflects finite-time hysteresis effects. The value of  $c_2$  is taken to be the average of these two estimates, and the difference between the two estimates provides a measure of the uncertainty in the determination of  $c_2$ . The phase boundary obtained this way is shown in Fig.13, along with the results for  $c_2(\lambda)$  obtained for the discrete model II from a similar analysis.

The general behavior found for all the models as the parameters  $\lambda$  and  $c$  are varied is qualitatively very similar to that in equilibrium first order phase transitions of two- and three-dimensional systems as the temperature and other parameters, such as the magnetic field in spin systems, are varied. To take a standard example of an equilibrium first order transition, we consider a system with a scalar order-parameter field  $\psi(\mathbf{r})$ , described by a Ginzburg-Landau free energy functional [39] that has a cubic term:

$$F[\psi] = \int d\mathbf{r} \left[ \frac{1}{2}a\psi^2(\mathbf{r}) - \frac{1}{3}b\psi^3(\mathbf{r}) + \frac{1}{4}u\psi^4(\mathbf{r}) \right], \quad (16)$$

where  $b$  and  $u$  are positive constants,  $a = a_0(T - T_0)$  with  $a_0 > 0$ , and  $T$  is the temperature. Considering uniform states,  $\psi(\mathbf{r}) = m$ , the free energy per unit volume may be written as

$$f(m) = \frac{1}{2}am^2 - \frac{1}{3}bm^3 + \frac{1}{4}um^4. \quad (17)$$

It is easy to show that for  $T_0 < T < T_s = T_0 + b^2/(4a_0u)$ , the function  $f(m)$  has two local minima, one at  $m = 0$ , and the other at a positive value of  $m$ . These two minima represent the two phases of the system. This system exhibits a first order equilibrium phase transition from the disordered phase ( $m = 0$ ) to an ordered phase with positive  $m$  as the temperature is decreased. The transition temperature  $T_c$  lies between  $T_0$  and  $T_s$ . The temperature  $T_s$  at which the minimum corresponding to the ordered phase disappears is called the “spinodal” temperature for the ordered phase. The spinodal temperature for the disordered phase is  $T_0$ .

Now consider the dynamics of this system according to the following time-dependent Ginzburg-Landau equation [39]:

$$\frac{\partial \psi(\mathbf{r}, t)}{\partial t} = -\Gamma \frac{\delta F[\psi]}{\delta \psi(\mathbf{r}, t)} + \eta(\mathbf{r}, t), \quad (18)$$

where  $\Gamma$  is a kinetic coefficient and  $\eta$  represents Gaussian delta-correlated noise whose variance is related to  $\Gamma$  and the temperature  $T$  via the fluctuation-dissipation theorem [39]. In the absence of noise, this equation converges to local minima of the functional  $F$ . So, the noiseless dynamics exhibits two locally stable fixed points for  $T_0 < T < T_s$ , corresponding to the two minima of  $f(m)$  that represent the disordered and uniformly ordered states. This is analogous to the two locally stable fixed points of our nonequilibrium dynamical systems for  $c < c_1(\lambda)$ . If we identify the flat and mounded fixed points as the “disordered” and “ordered” states, respectively, and the control parameter  $c$  to play the role of the temperature  $T$ , then the noiseless dynamics of our models would look similar to that of Eq.(18) for  $\eta = 0$ , with  $c_1$  playing the role of the spinodal temperature  $T_s$  of the equilibrium problem.

In the presence of noise, the system described by Eq.(18) exhibits a first-order phase transition at  $T_c$  that lies between  $T_s$  and  $T_0$ : the system selects one of the phases corresponding to the two fixed points of the noiseless dynamics, except at  $T_c$  where both phase coexist. The local stability of the mean-field ordered and disordered states in a small temperature-interval around  $T_c$  is manifested in the dynamics as finite-time hysteresis effects. The behavior we find for our nonequilibrium dynamical models is qualitatively similar: the system selects the steady state corresponding to the mounded (“ordered”) fixed point of the noiseless dynamics as the control parameter  $c$  (analogous to the temperature  $T$  of the equilibrium system) is decreased below  $c_2$  which is smaller than the “spinodal” value  $c_1$ . The growth models do not exhibit a “spinodal” point for the kinetically rough (“disordered”) phase: the flat fixed point of the noiseless dynamics is locally stable for all positive values



of the control parameter  $c$ . If this analogy with equilibrium first order transition is correct, then our models should show hysteresis and coexistence of kinetically rough and mounded morphologies for values of  $c$  near  $c_2(\lambda)$ . As mentioned above, we do find hysteresis (see inset of Fig.13) in finite-time simulations with values of  $c$  near  $c_2$ . Evidence for two-phase coexistence is presented in Fig.14, where a snapshot of the interface profile for a  $L = 500$  sample of model I with  $\lambda = 4.0$ ,  $c = 0.42$  is shown. This value of  $c$  is very close to the critical value  $c_2$  for  $\lambda = 4.0$  (see inset of Fig.13). This plot clearly illustrates the simultaneous presence of mounded and rough morphologies in the interface profile.

The results described above suggest that our growth models exhibit a *first-order dynamical phase transition* at  $c = c_2(\lambda)$ . To make this conclusion more concrete, we need to define an *order parameter*, analogous to the quantity  $m$  in the equilibrium problem discussed above, that is zero in the kinetically rough phase, and jumps to a non-zero value as the system undergoes a transition to the mounded phase at  $c = c_2$ . The identification of such an order parameter would also be useful for distinguishing between these two different kinds of growth in experiments – as mentioned in the Introduction, it is difficult to experimentally differentiate between kinetic roughening and mound formation with coarsening from measurements of the usual bulk properties of the interface. A clear distinction between the two morphologies may be obtained from measurements of the average number of extrema of the height profile [40]. The steady-state profile in the mound-formation regime exhibits two extrema for *all* values of the system size  $L$ . In contrast, the number of extrema in the steady state in the kinetic roughening regime increases with  $L$  as a power law [40] – we find that for values of  $c$  for which the system is kinetically rough, e.g. for  $\lambda = 4.0$ ,  $c = 0.05$  for model I, the average number of extrema in the steady state is proportional to  $L^\delta$  with  $\delta \simeq 0.83$ . This observation allows us to define an “order parameter” that is zero in the large- $c$ , kinetic roughening regime and finite in the small- $c$ , mound-formation regime. Let  $\sigma_i$  be an Ising-like variable, equal to the sign of the slope of the interface at site  $i$ . An extremum in the height profile then corresponds to a “domain wall” in the configuration of the  $\{\sigma_i\}$  variables. Since there are two domain walls separated by  $\sim L/2$  in the steady state in the mound-formation regime, the quantity

$$m = \frac{1}{L} \left| \left\langle \sum_{j=1}^L \sigma_j e^{2\pi i j/L} \right\rangle \right|, \quad (19)$$

where  $\langle \dots \rangle$  represents a time-average in the steady state, would be finite in the  $L \rightarrow \infty$  limit. On the other hand,  $m$  would go to zero for large  $L$  in the kinetically rough regime because the number of domains in the steady-state profile would increase with  $L$ . We find numerically that in the kinetically rough phase,  $m \sim L^{-\gamma}$  with

$\gamma \simeq 0.2$ . The finite-size scaling data for the order parameter  $m$  for models I and II for both faceted and kinetically rough phases is shown in Fig.15. It is seen that  $mL$  varies linearly with the system size  $L$  in the mounded phase, whereas  $mL \sim L^{1-\gamma}$  with  $\gamma \simeq 0.2$  for model I and  $\gamma \simeq 0.15$  for model II in the kinetically rough phase. So, in the  $L \rightarrow \infty$  limit, the order parameter would jump from zero to a value close to unity as  $c$  is decreased below  $c_2(\lambda)$ . This is exactly the behavior expected at a first-order phase transition.

The occurrence of a first-order phase transition in our 1d models with short-range interactions may appear surprising – it is well-known [39] that 1d systems with short-range interactions do not exhibit any equilibrium thermodynamic transition at a non-zero temperature. The situation is, however, different for nonequilibrium phase transitions: In contrast to equilibrium systems, a first-order phase transition may occur in one-dimensional nonequilibrium systems with short-range interactions. Several such transitions have been well documented in the literature [41]. So, there is no reason to *a priori* rule out the occurrence of a true first-order transition in our 1d nonequilibrium systems. As discussed above, our numerical results strongly suggest the existence of a true phase transition. However, since all our results are based on finite-time simulations of finite-size systems, we can not claim to have established rigorously the occurrence of a true phase transition in our models. The crucial question in this context is whether the order parameter  $m$  would be nonzero in the mounded phase in the  $L \rightarrow \infty$  limit if the time-average in Eq.(19) is performed over arbitrarily long times. Since the steady-state profile in this phase has a single mound and a single trough (this is clear from our simulations), the only way in which  $m$  can go to zero is through strong “phase fluctuations” corresponding to lateral shifts of the positions of the peak and the trough. We do not find any evidence for such strong phase fluctuations. We have calculated the time autocorrelation function of the phase of the order parameter for small samples over times of the order of  $10^7$  and found that it remains nearly constant at a value close to unity over the entire range of time. So, if such phase fluctuation eventually make the order parameter zero for all values of  $c$ , then this must happen over astronomically long times. Our finite-time simulations can not, of course, rule out this possibility.

## V. COARSENING OF MOUNDS

During the late-stage evolution of the interface, the mounds coarsen with time, increasing the typical size of the triangular pyramidal structures. The process of coarsening occurs by larger mounds growing larger at the expense of the smaller ones while always retaining their “magic” slope. Snapshots of the system in the coarsening regime are shown in Figs 16 and 17 for model I and

model II, respectively. The constancy of the slope during the coarsening process is clearly seen in these figures. As discussed in the Introduction, the constancy of the slope implies that if the typical lateral size of a mound increases in time as a power law with exponent  $n$  ( $R(t) \propto t^n$ ), then the width of the interface would also increase in time as a power law with the same exponent ( $W(t) \propto t^\beta$  with  $\beta = n$ ). Therefore, the value of the coarsening exponent  $n$  may be obtained by measuring the width  $W$  as a function of time in the coarsening regime. In Fig.18, we show a plot of the width as a function of time for model I with  $\lambda = 4.0$ ,  $c = 0.02$ . It is clear from the plot that the time-dependence of the width is well-described by a power law with  $\beta = n = 0.34 \pm 0.01$ . A similar plot for the discrete model II with  $\lambda = 2.0$ ,  $c = 0.005$ , shown in Fig.19, also shows a power-law growth of the width in the long-time regime, but the value of the coarsening exponent obtained from a power-law fit to the data is  $\beta = n = 0.50 \pm 0.01$ , which is clearly different for the value obtained for model I. This is a surprising result: model II was originally defined [31] with the specific purpose of obtaining an atomistic realization of the continuum growth equation of Eq.(3), and earlier studies [31–33] have shown that the dynamical scaling behavior of this model in the kinetic roughening regime is the same as that of model I. Also, we have found in the present study that the dynamical phase transition in this model has the same character as that in model I. So, the difference in the values of the coarsening exponents for these two models is unexpected. As noted earlier, there is some evidence suggesting that the typical slope of the mounds in model II increases very slowly with time (see Fig.10). However, this “steepening”, if it actually occurs, is too slow to account for the large difference between the values of the coarsening exponents for models I and II.

In order to understand these numerical results, we first address the question of why the mounds coarsen with time. This problem has certain similarities with domain growth in spin systems [42]. Using the Ising variables  $\{\sigma_i\}$  defined in the preceding section, each height profile can be mapped to a configuration of Ising spins. The coarsening of mounds then corresponds to a growth of the typical size of domains of these Ising spins. There is, however, an important difference between the coarsening of mounds in our models and the usual domain growth problem [42] for Ising spins. Domain growth in spin systems is the process through which the system approaches equilibrium from an out-of-equilibrium initial state. The dynamics of this process may be understood in terms of arguments based on considerations of the free energy (at finite temperatures) or energy (at zero temperature). Such arguments do not apply to our nonequilibrium growth models. The reason for the coarsening of mounds in our models must be sought in the relative stability of different structures under the assumed dynamics and the effects of noise.

As discussed in the preceding section, the fixed point of Eq.(8) with one mound and one trough is locally sta-

ble for  $c < c_1(\lambda)$ . Since structures with several mounds and troughs approach this steady-state structure through the coarsening process, it is reasonable to expect that fixed points of the noiseless equation with more than one mounds and troughs would be unstable. We have numerically obtained fixed points of Eq.(8) with two mounds and troughs for different values of the sample size and the separation between the peaks of the two mounds. The slope of the mounds at these fixed points is found to be the same as that in the fixed point with one mound and one trough. We find that the stability matrix for such fixed points always has a real, positive eigenvalue, indicating that the structure is unstable and would evolve to the stable configuration with one mound and one trough. The magnitude of the positive eigenvalue of the stability matrix for two-mounded fixed points depends on the sample size, the separation between the peaks of the mounds and the relative heights of the mounds in a complicated way. We have not been able to extract any systematic quantitative information from these dependences. We find a qualitative trend indicating that the magnitude of the positive eigenvalue decreases as the separation between the peaks of the two mounds is increased. Since the time scale of the development of the instability of two-mounded structures is given by the inverse of the positive eigenvalue, this result is consistent with the expectation that the time required for two mounds to coalesce should increase with the separation between the mounds.

These results suggest that the coarsening of the mounds in model I reflects the instability of structures with multiple mounds and troughs. If this is true, then coarsening of mounds should be observed in this model even when the noise term in Eq.(8) is absent. To check this, we have carried out numerical studies of coarsening in the noiseless version of Eq.(8). In these studies, the time evolution of an initial configuration with a pillar of height  $h_0 > h_{min}(\lambda, c)$  at the central site of an otherwise flat interface is followed numerically in the presence of noise until the instability caused by the presence of the pillar is well developed. The profiles obtained for different realizations of the noise used in the initial time evolution are then used as initial configurations for coarsening runs without noise. The dotted line in Fig.18 shows the width versus time data obtained from this calculation. The coarsening exponent in the absence of noise is found to be the same ( $n \simeq 1/3$ ) as that of the noisy system, indicating that the coarsening in this model is driven by processes associated with the deterministic part of the growth equation.

We have examined the details of the process by which two mounds coalesce to form a single one. The different steps in this process are illustrated in the snapshots of interface profiles shown in Fig.17 where one can see how the two mounds near the center come together to form a single one as time progresses. First, the separation between the peaks of the mounds decreases with time. When this distance becomes sufficiently small, the “V”-shaped segment that separates the peaks of the mounds “melts” to

form a rough region with many spikes. This region of the interface then self-organizes to become the top part of a mound. Although the data shown in this figure were obtained for model II, it also represents quite closely the process of coalescence of mounds in models I and IA. An estimate of the time scale associated with the second part of this process, during which the “melted” region of the interface transforms into the top part of a mound, may be obtained in the following way. The absolute value of the closest-to-zero eigenvalue of the stability matrix for the single-mounded fixed point provides an estimate of the time scale over which configurations close to the fixed point evolve to the fixed point itself. In the inset of Fig.18, we have shown the dependence of the magnitude  $\kappa_m$  of the closest-to-zero eigenvalue for  $\lambda = 4.0$ ,  $c = 0.02$  on the system size  $L$ . The eigenvalue scales with the system size as  $L^{-3}$ , indicating that the time scale for the decay of fluctuations with length scale  $L$  is proportional to  $L^3$ . This is consistent with the observed value of the coarsening exponent,  $n \simeq 1/3$ , which indicates that the time scale  $\tau(x)$  for the coalescence of mounds separated by distance  $x$  is proportional to  $x^{1/n} \sim x^3$ .

We have found very similar behavior for the closest-to-zero eigenvalue of the stability matrix for the single-mounded fixed point of model IA in which a different form of the control function is used. Coarsening data for this model are shown in Fig.18. In this model, there is a long time interval between the onset of the instability and the beginning of power-law coarsening. During this time interval, the interface segments near the tall pillars formed at the instability organize themselves into triangular mounds. This process produces a plateau in the width versus time plot. Eventually, however, power-law coarsening with  $n \simeq 1/3$  is recovered, as shown by the dashed line in Fig.18. Since the onset of power-law coarsening in this model occurs at very late times, we could not get coarsening data for this model over a very wide time interval. Consequently, the calculated value of the coarsening exponent for this model is less accurate. However, our results show quite clearly that the “universal” features of the coarsening dynamics of models I and IA are the same.

Going back to the discrete model II, we first examined its coarsening dynamics in the absence of noise. The noiseless limit of this model is not well-defined in the sense that there is no explicit noise term that can be turned off. The stochasticity in this model arises from two sources: first, the randomness associated with the selection of the deposition site  $i$  (the quantity  $K_i(\{h_j\})$  defined in Eq.(9) is calculated at this site and at its nearest-neighbor sites); and second, the randomness in the selection of one of the two neighbors of site  $i$  in case of a tie in their values of  $K_i$ . In order to make the dynamics deterministic, we employ a parallel update scheme in which all the lattice sites,  $i = 1, \dots, L$ , are updated simultaneously instead of sequentially. This eliminates the stochasticity arising from the choice of the sequence in which the sites are updated. The randomness associated with the selec-

tion of a neighbor in case of a tie is eliminated by choosing the right neighbor if the serial number of the occurrence of a tie, measured from the beginning of the simulation, is even, and the left neighbor if the serial number is odd. With these modifications of the update rules, the system evolves in a perfectly deterministic way. To study coarsening in this deterministic version of model II, we prepare an initial structure with two identical mounds separated by distance  $x_0$ . The slope of these mounds is chosen to be equal to the “selected” value found in simulations of the original model. We then study the time evolution of this structure according to the parallel dynamics defined above, monitoring how the distance  $x$  between the peaks of the mounds changes with time  $t$ . We find that the value of  $x$  increases initially, in order to accommodate a slightly higher value of the selected slope for the parallel dynamics. After reaching a maximum value that is  $\sim 20\%$  higher than  $x_0$ , the distance  $x$  decreases with time, indicating that the noiseless dynamics leads to coarsening. Eventually, the two mounds coalesce into a single one and the system remains in the state with one mound and one trough at later times. The slope of the mounds remains constant during the coarsening process. Assuming power-law coarsening with exponent  $n$ , the separation  $x$  at time  $t$  is expected to have the form

$$x(t) = (x_0^{1/n} - Ct)^n, \quad (20)$$

where  $C$  is a constant. This form implies that the time  $\tau(x_0)$  required for the coalescence of two mounds separated by distance  $x_0$  is proportional to  $x_0^{1/n}$ . In Fig.20, we have shown the time dependence of  $x(t)$  for three different initial separations,  $x_0 = 80, 90$  and  $100$ , and fits of the data to the form of Eq.(20), yielding the result  $1/n = 2.9 \pm 0.1$ . Only the data for  $x$  at times larger than the time at which it returns to  $x_0$  after the initial increase are shown in the figure. From these observations, we conclude that the coarsening exponent in the zero-noise limit of model II is the same ( $n = 1/3$ ) as that found for the two versions of the continuum model. The observation that the coarsening exponent for the noisy version of model II is different from  $1/3$  then indicates that the effect of noise in the discrete model is *qualitatively different* from that in the continuum models. We discuss below a possible explanation of this behavior.

The fact that noiseless versions of all three models exhibit the same value of the coarsening exponent ( $n = 1/3$ ) suggests that the coarsening is driven by an effective attractive interaction between the peaks of neighboring mounds. The observed value of  $n$  suggests [43] that the this attractive interaction is proportional to  $1/x^2$  where  $x$  is the separation between the mound tips. This interaction would lead to the observed result,  $\tau(x) \propto x^3$ , in the noiseless limit if the rate of change of  $x$  with  $t$  is assumed to be proportional to the attractive force (“over-damped limit”). The presence of noise in the original growth model leads to a noise term in the equation of motion of the variable  $x$ , but the nature of this noise term

is not clear. Since the observed coarsening dynamics in the noisy model II ( $n \simeq 0.5$ ) suggests a similarity with random walks, we propose that the effective dynamics of the variable  $x$  is governed by the kinetic equation

$$\frac{dx}{dt} = -C/x^2 + \eta(t), \quad (21)$$

where  $\eta$  is a Gaussian, delta-correlated noise with zero mean and variance equal to  $2D$ . In this phenomenological description, the coarsening of a two-mounded structure in model II is mapped to a Brownian walk of a particle in an attractive potential field with an absorbing wall at the origin, such that the particle cannot escape once it arrives at the origin. The absorption of a particle at the origin corresponds to the coalescence of two mounds in the original height picture. Thus, in this reduced model, the quantity of interest is the typical first passage time  $\tau$  (i.e. the time taken by a particle to reach the origin) as a function of  $x_0$ , the initial distance of the particle from the origin. In the noiseless limit ( $D = 0$ ),  $\tau$  is equal to  $x_0^3/(3C)$ , and in the purely Brownian walk limit ( $C = 0$ ), the typical value of  $\tau$  should be of the order of  $x_0^2/D$ . Therefore, for sufficiently large values of  $x_0$ , random-walk behavior characterized by  $n = 1/2$  is expected. However, for relatively small values of  $x_0$ , the behavior should be dominated by the attractive interaction. Therefore, we expect that the dynamics described by Eq.(21) with nonzero  $C$  and  $D$  would exhibit a crossover from a noise dominated regime to an interaction dominated regime as the value of  $x_0$  is decreased. This crossover is expected to occur near  $x_0 = x_c \sim C/D$ , for which the values of  $\tau$  obtained from the two individual terms in Eq.(21) become comparable. We, therefore, propose a scaling form for the dependence of  $\tau$  on  $x_0$ :

$$\tau(x_0) = \frac{x_0^3}{3C} F\left(\frac{Dx_0}{C}\right) \quad (22)$$

where the scaling function  $F(z)$  has the following asymptotic dependence on its argument  $z$ :  $F(z) = 1$  for  $z \ll 1$  and  $F(z) \propto 1/z$  for  $z \gg 1$ . Our numerical study of the reduced model of Eq.(21) confirms the validity of this scaling ansatz. Note that for any nonzero value of  $D$ ,  $\tau(x_0)$  would be proportional to  $x_0^2$ , implying  $n = 1/2$ , for sufficiently large values of  $x_0$ .

To test the validity of this reduced description of the coarsening dynamics of the original model II with stochastic sequential updates, we have simulated the evolution of a two-mounded structure in this model. The two-mounded structure used in these simulations is identical to that used in the study of coarsening in the model with parallel updates. In these simulations also, the average value of  $x$  exhibits a small initial increase followed by a steady decrease. The initial growth of  $\langle x^2(t) \rangle - \langle x(t) \rangle^2$  with time is found to be linear, indicating the presence of a random additive noise in the effective equation of motion of  $x$ . Fig.21 shows the time dependence of  $\langle x(t) \rangle$  obtained from simulations of  $L = 500$  samples of model

II with  $\lambda = 2.0$ ,  $c = 0.005$ , and  $x_0 = 100$ . In this plot, the origin of time has been shifted to the point where  $\langle x \rangle$  returns to the initial value  $x_0 = 100$  after the small initial increase, and  $10^3$  units of simulation “time” (number of deposited layers) is taken to be the unit of  $t$ . The number of independent runs used in the calculation of averages is 800. The observed dependence of  $\langle x(t) \rangle$  on  $t$  can be described reasonably well by the reduced equation of Eq.(21) for appropriate choice of the values of the parameters  $C$  and  $D$ . As shown in Fig.21, the  $\langle x(t) \rangle$  calculated numerically from Eq.(21) with  $C = 285.0$  and  $2D = 0.3$  provides a good fit to the data obtained from simulations of the growth model. Due to the limited range of the simulation data, the values of  $C$  and  $D$  can not be determined very accurately from such fits: values of  $C$  in the range 250 – 300 and values of  $D$  in the range 0.1 – 0.5 (larger values of  $C$  have to be combined with smaller values of  $D$ ) provide reasonable descriptions of the simulation data. For such values of  $C$  and  $D$ , and  $x_0 \approx L$  where  $L = 10^3$  is the sample size used in the calculation of the coarsening exponent,  $Dx_0/C$  is of order unity, indicating that the effects of the noise term in Eq.(21) should be observed in the simulation data. We, therefore, conclude that the presence of an additive random noise term in the effective equation of motion for the separation between the peaks of neighboring mounds in model II is a plausible explanation for the observed value of the coarsening exponent,  $n = 1/2$ .

In view of this conclusion, it is interesting to enquire why the coarsening exponent  $n$  for models I and IA has the value  $1/3$  characteristic of dynamics governed by the deterministic interaction between mound tips. We can not provide a conclusive answer to this question. One possibility is that the additive random noise in the original growth equations for these models does not translate into a similar noise in the effective equation of motion for the separation of mound tips. A second possibility is that the equation of motion for the separation  $x$  for these models also has the form of Eq.(21), but the relative strength of the noise is much smaller, so that the crossover value  $x_c$  is much larger than the typical sample sizes used in our simulations. Under these circumstances, the dynamics of  $x$  would be governed by the interaction and  $\tau$  would be proportional to  $x_0^3$ , giving the value  $1/3$  for the coarsening exponent  $n$ . If the second explanation is correct, then one should observe a crossover from  $n = 1/3$  to  $n = 1/2$  in models I and IA as the sample size  $L$  is increased. We do not find any evidence for such a crossover in our simulations.

In passing, we note that the dynamics of the slope variables  $\{s_i\}$  is strictly conserved in the models studied here if periodic or fixed boundary conditions are used. Also, the deterministic part of the growth equations conserves the integrated height. The “magnetization” of the Ising variables  $\{\sigma_i\}$  representing the signs of  $\{s_i\}$  is not strictly conserved: it is conserved only in a statistical sense. However, unlike other well-known examples [42] of systems with conserved dynamics, we obtain in model

II a coarsening exponent that is different from the expected Lifshitz-Slyozov value,  $n = 1/3$ . Since the height variables in model II are integers, there are some sites for which  $h_i = h_{i+1}$ . The assignment of the value of the Ising variable  $\sigma_i$  at such sites is clearly ambiguous. It may be more appropriate to use a three-state variable, taking the values  $\pm 1$  and  $0$ , to describe the coarsening behavior of this model. This problem does not arise in models I and IA for which the height variables are real numbers because the likelihood of two neighboring height variables to be exactly the same is vanishingly small.

## VI. MODEL I WITH CONSERVED NOISE

As discussed in section IV, the properties of the mounded phase of model I are determined to a large extent by the mounded fixed point of the deterministic part of the equations of motion of the height variables. The presence of noise changes the critical value of the control parameter  $c$  from  $c_1$  to  $c_2 < c_1$ , but does not affect strongly the properties of the mounded steady state of the system (see, for example, Fig.11). Therefore, we expect that the properties of the mounded phase would not change drastically if the statistics of the noise is altered. On the other hand, it is well-known [1,2] that the exponents that describe the scaling behavior in the kinetically rough phase depend strongly on the nature of the noise. In particular, the exponents for conserved noise are expected to be quite different from those describing the behavior for nonconserved noise. The occurrence of the nonlinear instability that leads to the mounded phase in our models is contingent upon the spontaneous formation of pillars of height  $h_0 > h_{min}(\lambda, c)$ , if the initial state of the system is completely flat. The probability of formation of such pillars depends crucially [33] on the values of the roughening exponents which, in turn, are strongly dependent on the nature of the noise. Therefore, we expect that the nature of the noise may be very important in determining whether the instability leading to mound formation actually occurs in samples with flat initial states.

We have investigated this issue in detail by carrying out simulations of a version of Model I in which the noise is conserved [35]. The equations of motion for the height variables in this model have the form of Eq.(8), with the noise terms  $\{\eta_i(t)\}$  having the properties

$$\langle \eta_i(t) \rangle = 0, \quad \langle \eta_i(t) \eta_j(t') \rangle = -\tilde{\nabla}^2 \delta_{i,j} \delta_{t,t'}, \quad (23)$$

where  $\delta_{ij} = 1$  if  $i = j$  and zero otherwise. This model is expected to exhibit kinetic roughening with exponents  $\beta \simeq 1/11$ ,  $\alpha \simeq 1/3$ , and  $z \simeq 11/3$  in one dimension [35]. Since the value of  $\alpha$  for this model is less than unity, it exhibits conventional dynamical scaling with the typical value of the nearest-neighbor height difference saturating at a constant value at long times. The value of this constant is expected to increase [33] as the strength  $\lambda$  of

the nonlinearity is increased. As discussed in detail in Ref. [33], the nonlinear instability that leads to mound formation is expected to occur in the time evolution of such models from a perfectly flat initial state only if the value of  $\lambda$  is sufficiently large to allow the spontaneous, noise-induced formation of pillars of height greater than  $h_{min}(\lambda, c)$ . So, if the value of  $\lambda$  is sufficiently small, then the model with conserved noise, evolving from a flat initial state, would not exhibit the mounding transition. On the other hand, if the instability is induced in the model by starting the time evolution from a state in which there is at least one pillar with height greater than  $h_{min}$ , then it is expected to evolve to the mounded state if the value of  $c$  is sufficiently small to make the mounded state stable. So, the long-time steady state of the conserved model is expected to exhibit an interesting dependence on the initial state: if  $\lambda$  is sufficiently small (so that pillars with height greater than  $h_{min}$  are not spontaneously generated in the time evolution of the interface from a flat initial state), and the value of  $c$  sufficiently small (so that the mounded state is stable in the presence of noise), then the steady state would be kinetically rough if the initial state is sufficiently smooth, and mounded if the initial state contains pillars of height greater than  $h_{min}$ . This ‘‘bistability’’ does not occur for the nonconserved model I because the nearest-neighbor height difference in this model continues to increase with time, so that the instability always occurs at sufficiently long times [33].

Our simulations of the model with conserved noise show the bistable behavior discussed above in a large region of the  $c - \lambda$  plane. We find that in this model, the height of a pillar on an otherwise flat interface increases in time if its initial value  $h_0$  is larger than  $h_{min} \simeq 20/\lambda$  (the dependence of  $h_{min}$  on  $c$  is weak). This dependence of  $h_{min}$  on  $\lambda$  is very similar to that [33] found for model I with nonconserved noise. We also find that the typical values of the nearest-neighbor height difference do not continue to increase with time in this model. Consequently, if  $\lambda$  is sufficiently small, pillars with height greater than  $h_{min}$  are not generated, and the system exhibits conventional kinetic roughening with exponent values close to the expected ones [35]. On the other hand, if the time evolution of the same system is started from a state with a pillar of height greater than  $h_{min}$ , then it evolves to a mounded state very similar to the one found in the model with nonconserved noise if the value of  $c$  is sufficiently small. The two steady states obtained for the conserved model with  $\lambda = 4.0$ ,  $c = 0.01$  are shown in Fig.22. The long-time state obtained in a run starting from a flat configuration is kinetically rough, whereas the state obtained in a run in which the nonlinear instability is initially seeded in the form of a single pillar of height  $h_0 = 1000$  at the central site is mounded with a well-defined slope, as in model I with nonconserved noise. The difference between the two profiles, obtained for the same parameter values for two different initial states, is quite striking.

Since the steady state in the conserved model depends on the initial condition, it is not possible to draw a conventional phase diagram for this model in the  $c-\lambda$  plane: the transition lines are different for different initial conditions. In Fig.23, we have shown three transition lines for this model in the  $c-\lambda$  plane. The line drawn through the circles (line 1) is obtained from simulations in which the system is started from a flat initial state. If  $\lambda$  is small, then the steady state reached in such runs is kinetically rough for all values of  $c$ . As  $\lambda$  is increased above a “critical value”  $\lambda_c \simeq 5.3$ , pillars with height greater than  $h_{min}$  are spontaneously generated during the time evolution of the system and it exhibits a transition to the mounded state if the value of  $c$  is not very large. The circles represent the values of  $c$  for which 50% of the runs show transitions to the mounded state. The line through the diamonds (line 2) corresponds to 50% probability of transition to the mounded state from an initial state with a pillar of height  $h_0 = 1000$  on an otherwise flat interface. The probability of reaching a mounded steady state in such runs decreases from unity as the value of  $c$  is increased, and falls below 50% as line 2 is crossed from below. For large  $\lambda$ , lines 1 and 2 merge together. This is expected: the probability of occurrence of a mounded steady state should not depend on how the pillars that initiate the nonlinear instability are generated. The third line (the one passing through the squares) represents 50% probability of transition to the kinetically rough state from a mounded initial state (the fixed point of the noiseless equations of motion with one mound and one trough). This line reflects the noise-induced instability of the mounded steady state for relatively large values of  $c$ . The differences between lines 2 and 3 are due to finite-time hysteresis effects similar to those discussed in section IV in the context of determining the critical value  $c_2(\lambda)$  of the control parameter  $c$  for model I with nonconserved noise.

The interesting region in the “phase diagram” of Fig.23 is the area enclosed by lines 1 and 2 and the  $c = 0$  line. For parameter values in this region, the system exhibits bistable behavior, as discussed above. This bistability is unexpected in the sense that in most studies of nonequilibrium surface growth, it is implicitly assumed that the long-time steady state of the system does not depend on the choice of the initial state. So, it is important to examine whether the dependence of the steady state on the initial condition in the conserved model reflects a very long (but finite) transition time from one of the two apparent steady states to the other one. We have addressed this question by carrying out long ( $t$  of the order of  $10^7$ ) simulations of small samples with parameter values in the middle of the “bistable region” for flat and mounded initial states. We did not find any evidence for transitions from one steady state to the other one in such simulations. Of course, we can not rule out the possibility that such transitions would occur over much longer time scales.

To summarize, we have shown from numerical simulations that a class of 1d surface growth models exhibits mound formation and power-law coarsening of mounds with slope selection as a result of a nonlinear instability that is controlled by the introduction of an infinite series of terms with higher-order gradient nonlinearities. The models considered here are discretized versions of a well-known continuum growth equation and an atomistic model originally formulated for providing a discrete realization of the growth equation. We have shown that these models exhibit a dynamical phase transition between a kinetically rough phase and a mounded phase as a parameter that measures the effectiveness of controlling the instability is varied. We have defined an order parameter for this first-order transition and used finite-size scaling to demonstrate how the sample-size dependence of this order parameter provides a clear distinction between the rough and mounded phases. We have also mapped out the phase boundary that separates the two phases in a two-dimensional parameter space.

We would like to emphasize that the ES mechanism, commonly believed to be responsible for mound formation in surface growth, is not present in our models. Our models exhibit a nonlinear instability, instead of the linear instability used conventionally to represent the effects of ES barriers. The mechanism of mound formation in our models is also different from a recently discovered [17,18] one involving fast edge diffusion, which occurs in two or higher dimensions. The slope selection found in our models is a rare example of pattern formation from a nonlinear instability. This is clearly different from slope selection in ES-type models in which the mounds maintain a constant slope during coarsening only if the nonequilibrium surface current vanishes at a particular value of the slope. The selected slope in such models is simply the slope at which the current is zero. The behavior of our models is more complex: in these models, the surface current is zero for all values of constant slope, and the selected value of the slope is obtained from a nonlinear mechanism of pattern selection.

Our studies bring out two other unexpected results. We find that the coarsening behavior of an atomistic model (model II) specifically designed to provide a discrete realization of the growth equation that leads to model I is different from that of model I: the exponents that describe the power-law coarsening are different in the two models. We show that this difference may arise from a difference in the nature of the effective noise that enters the equation of motion for the separation between neighboring mounds in the two cases. The second surprising result is that the numerically obtained long-time behavior of model I with conserved noise in a region of parameter space depends crucially on the initial conditions: the system reaches a mounded or kinetically rough

steady state depending on whether or not the initial state is sufficiently rough. To our knowledge, this is the first example of “nonergodic” behavior in nonequilibrium surface growth.

The behavior found in our 1d models may be relevant to experimental studies of the roughening of steps on a vicinal surface. As noted earlier, the form of the control function  $f(x)$  used in model IA is physically reasonable. However, since very little is known about the values of the model parameters appropriate for experimentally studied systems, we are unable to determine whether the mechanism of mound formation found in our study would be operative under experimentally realizable conditions. The nonlinear instability found in our 1d models is also present [34] in the experimentally interesting two-dimensional version of the growth equation of Eq.(3). However, it is not clear whether this instability, when controlled in a manner similar to that in our 1d models, would lead to the formation of mounds in two dimensions. This question is currently under investigation. Since the growth equation of Eq.(3) exhibits conventional dynamic scaling in the kinetic roughening regime in two dimensions, the nonlinear instability would not occur in runs with flat initial states if the value of  $\lambda$  is small. Therefore, the behavior in two dimensions is expected to be similar to that of our 1d model I with conserved noise: the nature of the long-time steady state may depend crucially on initial conditions in a region of parameter space. Such nonergodic behavior, if found in two dimensions, would have interesting implications for the growth of films on patterned substrates.

All the results described in this paper have been obtained from numerical studies of models that are discrete in both space and time. It is interesting to enquire whether the truly continuum growth equation of Eq.(3) exhibits similar behavior. This question acquires special significance in view of studies [33,44] that have shown that discretization may drastically change the behavior of nonlinear growth equations similar to Eq.(3). Since the interesting behavior found in our discretized models arises from the nonlinear instability found earlier [32,33], the question that we have to address is whether a similar instability is present in the truly continuum growth equation. This question was addressed in some detail in Ref. [33] where it was shown that the nonlinear instability is not an artifact of discretization of time or the use of the simple Euler scheme for integrating the growth equation. In the present study, we have found additional evidence (see section III) that supports this claim. We should also point out that the atomistic model II, for which the question of inaccuracies arising from time integration does not arise, exhibits very similar behavior, suggesting that the behavior found in models I and IA is not an artifact of the time discretization used in the numerical integration.

The occurrence of the nonlinear instability does depend on the way space is discretized (i.e. how the lattice derivatives are defined). In earlier work [32,33] as well

as in the present study, the lattice derivatives are defined in a left-right symmetric way. We have found that the instability actually becomes stronger if the number of neighbors used in the definition of the lattice derivatives is increased. This result suggests that the instability is also present in the continuum equation. It has been found by Putkaradze *et al.* [45] that the instability does not occur if the lattice derivatives are defined in a different way in which either left- or right-discretization of the nonlinear term is used, depending on the sign of the local slope of the interface. There is no reason to believe that this definition is “better” or “more physical” than the symmetric definitions used in our work. The only rigorous result we are aware of for the behavior of Eq.(3) is derived in Ref. [45] where it is shown that the solutions of the noiseless equation are bounded for sufficiently smooth initial conditions. This result, however, does not answer the question of whether the instability occurs in the continuum equation. As discussed in Ref. [33], the nonlinear instability of Eq.(4), signalled by a rapid initial growth of the height (depth) of isolated pillars (grooves), may not lead to a true divergence of the height variables. The results reported in the present work would remain valid as long as high pillars or deep grooves are formed by the instability – the occurrence of a true divergence is not necessary.

In the present work, we have shown (see section IV) that the continuum equation with  $f(x)$  defined in Eq.(10) does admit stationary solutions that exhibit all the relevant features of stationary solutions of the discretized equation. This result provides additional support to the contention that the behaviors of the continuum and discretized systems are qualitatively similar. We should, however, mention that these stationary solutions of the continuum equation do not pick out a selected slope of the interface: profiles similar to those shown in Fig.11 may be obtained for different values of the parameter  $A$  in Eq.(14) that determines the slope of the triangular mound. Slope selection in the continuum equation may occur as a consequence of the requirement of local stability of such stationary solutions. As mentioned in section IV, we have not attempted a linear stability analysis of such numerically obtained stationary solutions of the continuum equation because doing such a calculation without discretizing space would be extremely difficult. Further investigation of this question would be useful.

Finally, we would like to emphasize that the discrete models studied here would continue to be valid models for describing nonequilibrium surface growth even if the behavior of the truly continuum growth equation of Eq.(3) turns out to be different from that found here. These models may be looked upon as ones in which continuous (in models I and IA) or discrete (in model II) height variables defined on a discrete lattice evolve in continuous or discrete time. These models have all the correct symmetries and conservation laws of the physical problem, and they exhibit, for different values of the control parameter  $c$ , both the phenomena of kinetic roughening

and mound formation found in experiments. There is no compelling reason to consider the continuum equation to be more “correct” or “physical” than these models. Epitaxial growth is intrinsically a discrete process at the molecular level and a continuum description is an approximation that may not be valid in some situations.

From a different perspective, the nonequilibrium first-order phase transition found in our models is interesting, especially because it occurs in 1d systems with short range interactions. Such phase transitions have been found earlier in several 1d “particle hopping” models [41]. It would be interesting to explore possible connections between such models and the 1d growth models studied here.

### VIII. ACKNOWLEDGEMENT

We thank SERC, IISc for computational facilities, and S. Das Sarma and S. S. Ghosh for useful discussions.

---

\* Currently at the Department of Physics, Condensed Matter Theory Center, University of Maryland, College Park, MD 20742.

[1] A.-L. Barabasi and H. E. Stanley, *Fractal Concepts in Surface Growth* (Cambridge University Press, Cambridge, 1995).

[2] J. Krug, *Adv. Phys.* **46**, 139 (1997).

[3] J. Krim and G. Palasantzas, *Int. J. Mod. Phys.* **B9**, 599 (1997).

[4] M. D. Johnson, C. Orme, A. W. Hunt, D. Graff, J. Sudijono, L. M. Sander and B. G. Orr, *Phys. Rev. Lett.* **72**, 116 (1994).

[5] K. Thurmer, R. Koch, M. Weber and K. H. Rieder, *Phys. Rev. Lett.* **75**, 1767 (1995).

[6] J. A. Stroschio, D. T. Pierce, M. Stiles, A. Zangwill and L. M. Sander, *Phys. Rev. Lett.* **75**, 4246 (1995).

[7] F. Tsui, J. Wellman, C. Uher and R. Clarke, *Phys. Rev. Lett.* **76**, 3164 (1996).

[8] J.-K. Zuo and J. F. Wendelken, *Phys. Rev. Lett.* **78**, 2791 (1997).

[9] M. F. Gyure, J. K. Zinck, C. Ratsh and D. D. Vvendsky, *Phys. Rev. Lett.* **81**, 4931 (1998).

[10] G. Apostolopoulos, J. Herfort, L. Dameritz and K. H. Ploog, *Phys. Rev. Lett.* **84**, 3358 (2000).

[11] Y.-P. Zhao, H.-N. Yang, G.-C. Wang and T.-M. Lu, *Phys. Rev. B* **57**, 1922 (1998).

[12] G. Lengel, R. J. Phaneuf, E. D. Williams, S. Das Sarma, W. Beard and F. G. Johnson, *Phys. Rev. B* **60**, R8469 (1999).

[13] M. Siegert and M. Plischke, *Phys. Rev. Lett.* **73**, 1517 (1994).

[14] M. Rost and J. Krug, *Phys. Rev. E* **55**, 3952 (1997).

[15] M. Siegert, *Phys. Rev. Lett.* **81**, 5481 (1998).

[16] L. Golubovic, *Phys. Rev. Lett.* **78**, 90 (1997).

[17] O. Pierre-Louis, M. R. D’Orsogna and T. L. Einstein, *Phys. Rev. Lett.* **82**, 3661 (1999).

[18] M. V. Ramana Murty and B. H. Cooper, *Phys. Rev. Lett.* **83**, 352 (1999).

[19] S. Das Sarma and P. Punyindu, *Surf. Sci. Lett.* **424**, L339 (1998).

[20] M. Biehl, W. Kinzel, and S. Schinzer, *Europhys. Lett.* **41**, 443 (1998).

[21] J. Krug, *J. Stat. Phys.* **87**, 505 (1997).

[22] I. Elkinani and J. Villain, *J. Phys. I* **4**, 949 (1994).

[23] P. Politi and J. Villain, *Phys. Rev. B* **54**, 5114 (1996).

[24] S. Das Sarma, P. Punyindu and Z. Toroczkai, *Surf. Sci. Lett.* **457**, L309 (2000).

[25] P. Punyindu-Chatraphorn, Z. Toroczkai and S. Das Sarma, *Phys. Rev. B* **64**, 205407 (2001).

[26] S. Das Sarma, S. V. Ghaisas, and J. M. Kim, *Phys. Rev. E* **49**, 122 (1994).

[27] G. Ehrlich and F. G. Hudda, *J. Chem. Phys.* **44**, 1039 (1996); S. C. Wang and G. Ehrlich, *Phys. Rev. Lett.* **70**, 41 (1993).

[28] R. L. Schwoebel and E. J. Shipsey, *J. Appl. Phys.* **37**, 3682 (1966); R. L. Schwoebel, *J. Appl. Phys.* **40**, 614 (1969).

[29] J. Villain, *J. Phys. I (France)* **1**, 19 (1991).

[30] Z. W. Lai and S. Das Sarma, *Phys. Rev. Lett.* **66**, 2348 (1991).

[31] J. M. Kim and S. Das Sarma, *Phys. Rev. Lett.* **72**, 2903 (1994).

[32] C. Dasgupta, S. Das Sarma, and J. M. Kim, *Phys. Rev. E* **54**, R4552 (1996).

[33] C. Dasgupta, J. M. Kim, M. Dutta, and S. Das Sarma, *Phys. Rev. E* **55**, 2235 (1997).

[34] A. Kundagrami and C. Dasgupta, *Physica A* **270**, 135 (1999).

[35] T. Sun, H. Guo, and M. Grant, *Phys. Rev. A* **40**, 6763 (1989).

[36] B. Chakrabarti and C. Dasgupta, *Europhys. Lett.* (in press).

[37] L. F. Shampine, *Numerical Solution of Ordinary Differential Equations* (Chapman & Hall, New York, 1994).

[38] Z. Racz, M. Siegert, D. Liu and M. Plischke, *Phys. Rev. A* **43**, 5275 (1991).

[39] S.-K. Ma, *Modern Theory of Critical Phenomena* (Benjamin, Reading, 1976).

[40] Z. Toroczkai, G. Corniss, S. Das Sarma and R. K. P. Zia, *Phys. Rev. E* **62**, 276 (2000).

[41] M. R. Evans, *Brazilian J. Phys.* **30**, 42 (2000) [condmat/0007293].

[42] A. J. Bray, *Adv. Phys.* **43**, 357 (1994).

[43] A. D. Rutenberg and A. J. Bray, *Phys. Rev. E* **50**, 1900 (1994).

[44] T. Newmann, and A. J. Bray, *J. Phys. A* **29**, 7917 (1996).

[45] V. Putkaradze, T. Bohr and J. Krug, *Nonlinearity* **10**, 823 (1997).



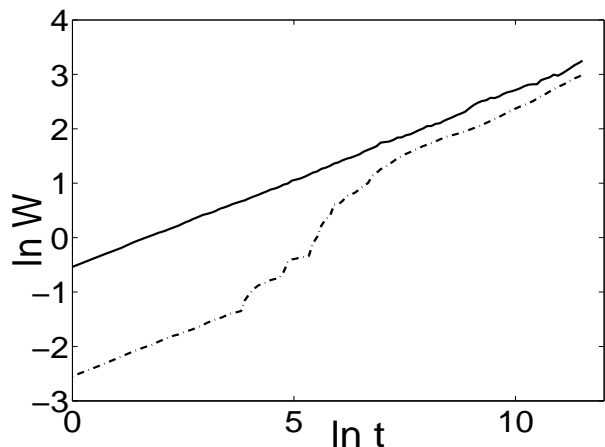


FIG. 1. Double-log plots of the interface width  $W$  as a function of time  $t$  for model I with  $\lambda = 4.0$ ,  $c = 0.02$  (dash-dotted line), and for  $\lambda = 4.0$ ,  $c = 0.06$  (full line). These data are for  $L = 500$  samples, averaged over 40 independent runs starting from flat initial states. Plots have been shifted vertically for clarity.

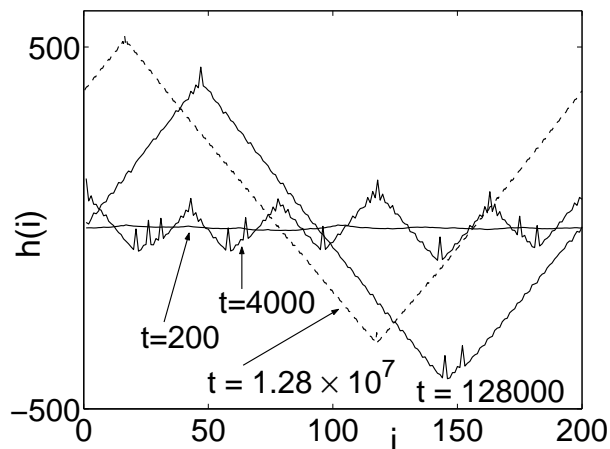


FIG. 3. The interface profile at three different times ( $t = 200$ , 4000, and 128000) in a run starting from a flat state for a  $L = 200$  sample of model I with  $\lambda=4.0$  and  $c=0.02$ . The dashed line shows the profile for a  $L = 500$  sample with the same parameters at  $t = 1.28 \times 10^7$ , with both axes scaled by 2.5.

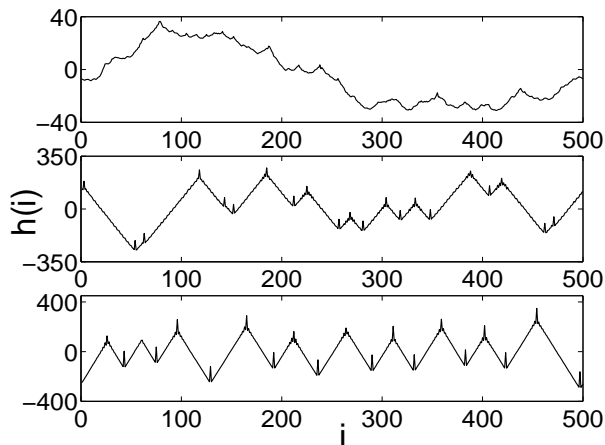


FIG. 2. Configuration snapshots at  $t=10^5$ , for model I with  $\lambda=4.0$ ,  $c=0.06$  (top panel), model I with  $\lambda=4.0$ ,  $c=0.02$  (middle panel), and model IA with  $\lambda=4.0$ , and  $c=0.01$  (bottom panel).

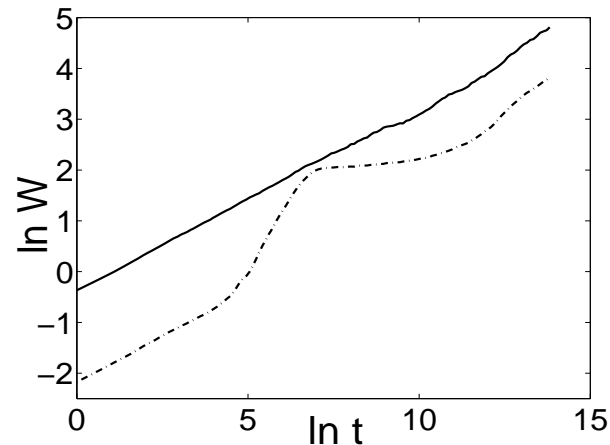


FIG. 4. Double-log plots of the interface width  $W$  as a function of time  $t$  for model II with  $\lambda=2.0$ ,  $c=0.005$  (dash-dotted line), and for  $\lambda=2.0$ ,  $c=0.015$  (full line). These data are for  $L = 500$  samples, averaged over 40 independent runs starting from flat states. Plots have been shifted vertically for clarity.

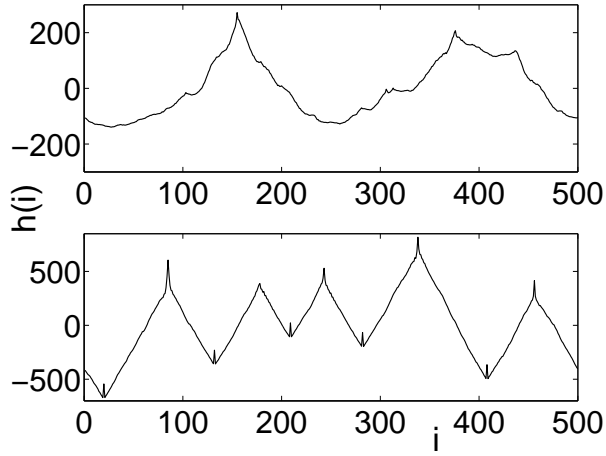


FIG. 5. Configuration snapshots at  $t=10^6$  for model II with  $\lambda=2.0$ ,  $c=0.015$  (top panel), and  $\lambda=2.0$ ,  $c=0.005$  (bottom panel).

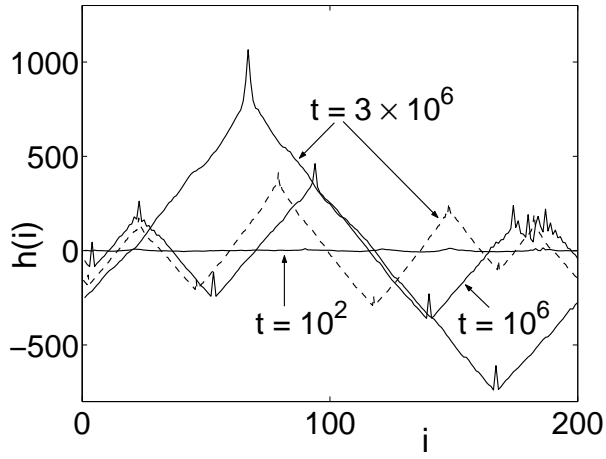


FIG. 6. The interface profile at three times ( $t = 10^2$ ,  $10^6$ , and  $3 \times 10^6$ ) in a run starting from a flat state for a  $L = 200$  sample of model II with  $\lambda=2.0$  and  $c=0.005$ . The profile of a  $L = 500$  sample with the same parameters at  $t = 3 \times 10^6$ , with both axes scaled by 2.5, is shown by the dashed line.

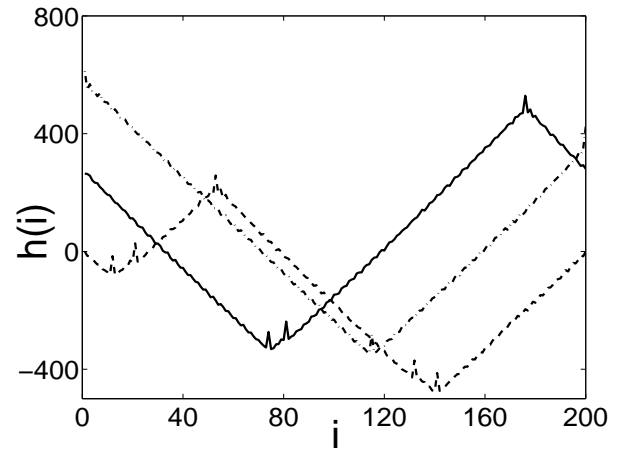


FIG. 7. Height profiles for model I ( $\lambda = 4.0$ ,  $c = 0.02$ ) at time  $t = 1.28 \times 10^7$  for periodic boundary conditions (full line), fixed boundary conditions (dashed line), and zero-flux boundary conditions (dash-dotted line).

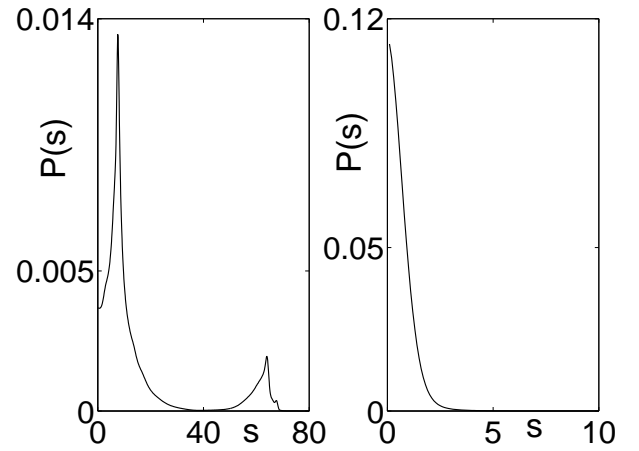


FIG. 8. Distribution of the magnitude of the nearest-neighbor height difference  $s$  for model I with  $\lambda=4.0$  and  $c=0.02$  (left panel), showing the bimodal nature of the distribution, characteristic of a mounded phase with slope selection. The distribution for  $\lambda=4.0$ ,  $c=0.05$  (right panel) does not show this behavior.

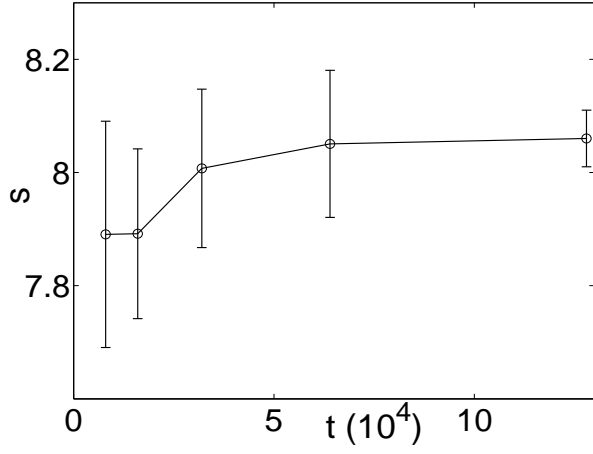


FIG. 9. Average slope of the mounds as a function of time for model I in the mounded phase ( $\lambda = 4.0$ ,  $c = 0.02$ ) during the coarsening process,  $t=8000$  to  $t=1.28 \times 10^5$ . The data are for  $L=500$  samples averaged over 40 runs.

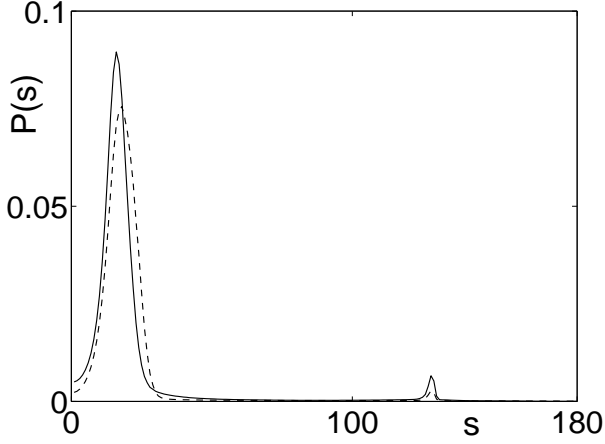


FIG. 10. Distribution of the magnitude of the nearest-neighbor height difference  $s$  for model II with  $\lambda=2.0$  and  $c=0.005$ , at two different times,  $t=10^6$  (full line) and  $t=10^7$  (dashed line).

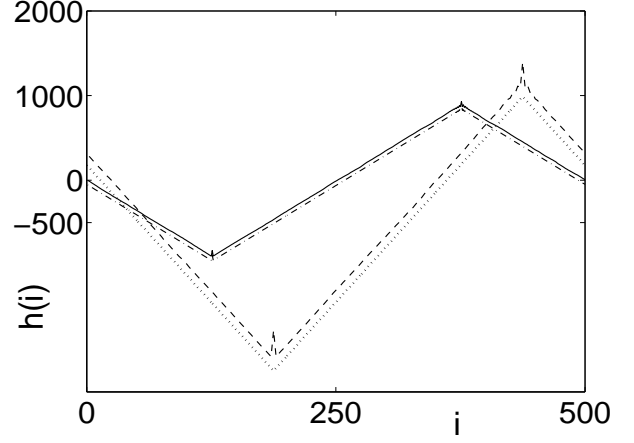


FIG. 11. Fixed point profile for a  $L = 500$  sample of model I with  $\lambda=4.0$  and  $c=0.02$  (full line), compared with a steady state profile (dash-dotted line) for the same parameter values. The dashed line shows a steady state profile of a  $L = 200$  sample of model IA with  $\lambda = 4.0$ ,  $c = 0.01$  (both axes scaled by 2.5), and the dotted line shows an invariant solution of the corresponding continuum equation.

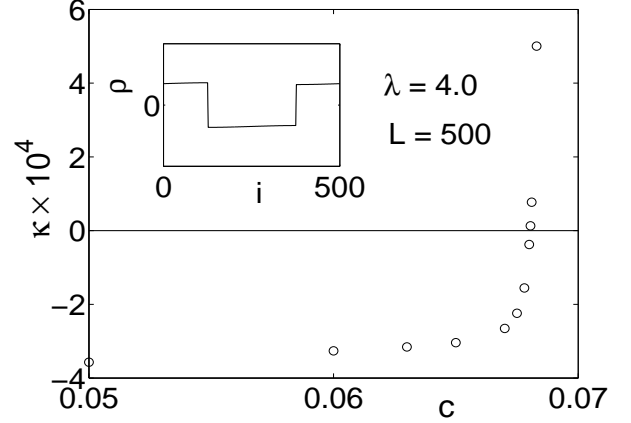


FIG. 12. The dependence of  $\kappa$ , the closest-to-zero eigenvalue of the stability matrix for the mounded fixed point of model I with  $\lambda=4.0$ ,  $L=500$ , on the control parameter  $c$ . The inset shows the right eigenvector  $\rho_i$  corresponding to this eigenvalue near the point where  $\kappa$  crosses zero.

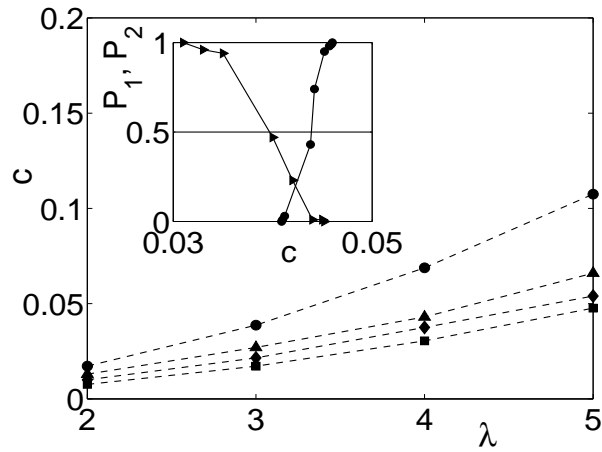


FIG. 13. Critical values of the control parameter  $c$  as functions of  $\lambda$ :  $c_1$  of model I (circles),  $c_2$  of model I (triangles),  $c_2$  of model II (diamonds), and  $c_1$  of model IA (squares). Inset: The probabilities  $P_1$  (circles) and  $P_2$  (triangles) defined in text, as functions of  $c$  for model I with  $\lambda = 4.0$ ,  $L = 200$ .

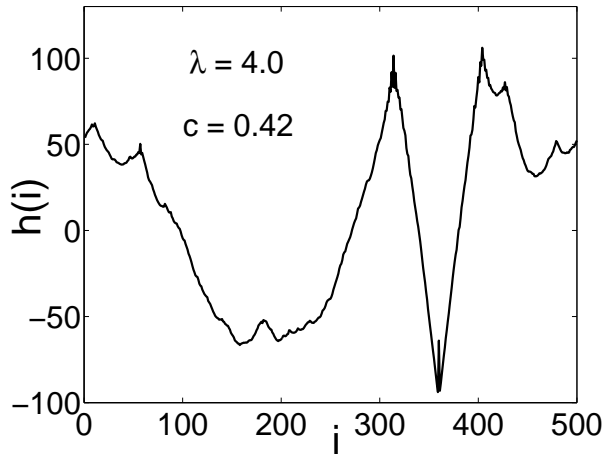


FIG. 14. Two phase coexistence near the phase transition in model I. The plot shows an interface profile of a  $L = 500$  sample with  $\lambda=4.0$ ,  $c=0.42$ .

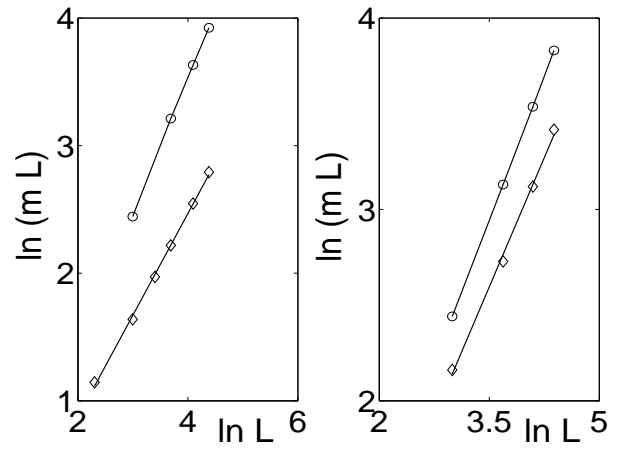


FIG. 15. Finite-size scaling for the order parameter  $m$ . The left panel shows double-log plots of  $mL$  as a function of the sample size  $L$  for model I in the mounded phase ( $\lambda=4.0$ ,  $c=0.02$ , circles) with slope  $1.00 \pm 0.01$  and in the kinetically rough phase ( $\lambda=4.0$ ,  $c=0.05$ , diamonds) with slope  $0.81 \pm 0.02$ . The right panel shows similar plots for model II in the mounded phase ( $\lambda=2.0$ ,  $c=0.005$ , circles) with slope  $1.00 \pm 0.01$  and in the kinetically rough phase ( $\lambda=2.0$ ,  $c=0.015$ , diamonds)  $0.88 \pm 0.02$ . The straight lines are the best power-law fits to the data.

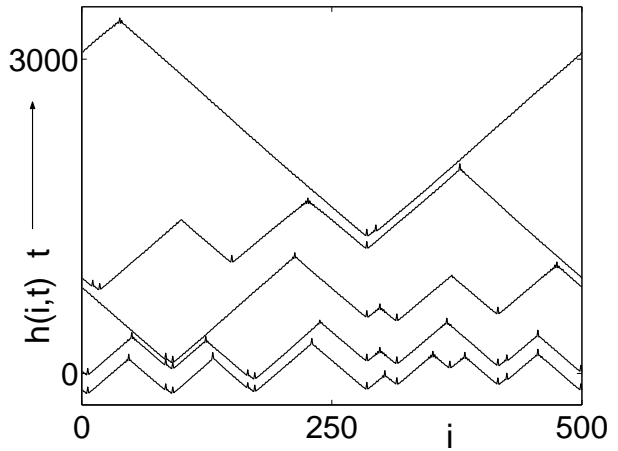


FIG. 16. Snapshots ( $t = 2 \times 10^4$ ,  $6 \times 10^4$ ,  $10^5$ ,  $1.4 \times 10^5$ , and  $1.28 \times 10^7$ ) of the profile of a  $L = 500$  sample of model I (profiles at different times have been shifted in the vertical direction for clarity) with  $\lambda=4.0$ ,  $c=0.02$  in the coarsening regime.

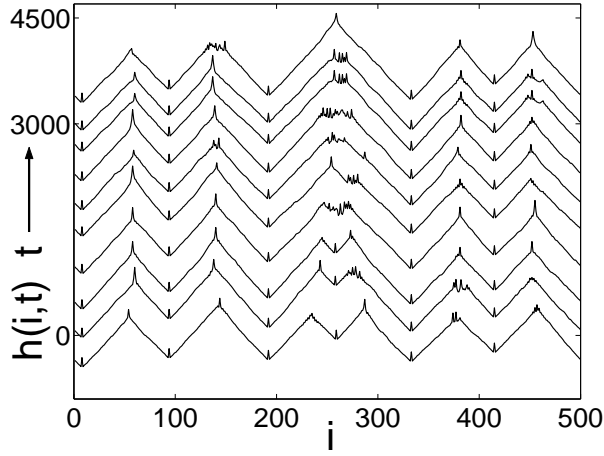


FIG. 17. Snapshots ( $t = 1100000, 1200000, 1250000, 1301000, 1450000, 1606000, 1660000, 1670000, 1680000, 1700000$ ) of the profile of a  $L = 500$  sample of model II (profiles at different times have been shifted in the vertical direction for clarity) with  $\lambda=2.0, c=0.005$  in the coarsening regime.

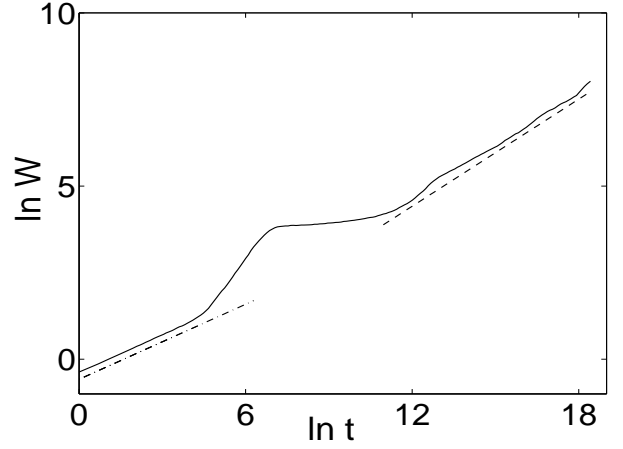


FIG. 19. Double-log plot of the interface width  $W$  as a function of time  $t$  for model II with  $\lambda=2.0$  and  $c=0.005$  (solid line) for  $L=1000$  samples averaged over 40 runs. The dash-dotted and dashed lines represent power-law behavior with exponent  $n = 1/3$  and  $n = 1/2$ , respectively.

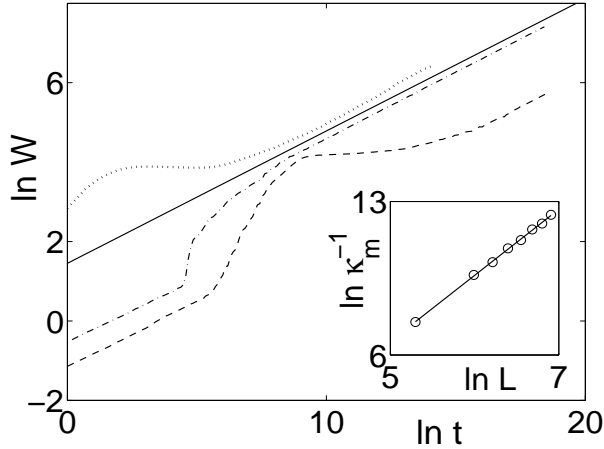


FIG. 18. Double-log plots of the interface width  $W$  as a function of time  $t$  for model I with  $\lambda=4.0$  and  $c=0.02$ , with noise (dash-dotted line), and without noise (dotted line) averaged over 40 runs for  $L = 1000$  samples. The dashed line shows  $W$  versus  $t$  data for model IA with  $\lambda=4.0, c=0.01$ , averaged over 60 runs for  $L = 500$  samples. The solid line represents power-law behavior with exponent  $n = 1/3$ . Inset: Finite-size scaling data for the inverse of the closest-to-zero eigenvalue of the stability matrix for the mounded fixed point of model I with  $\lambda = 4.0, c = 0.02$ .

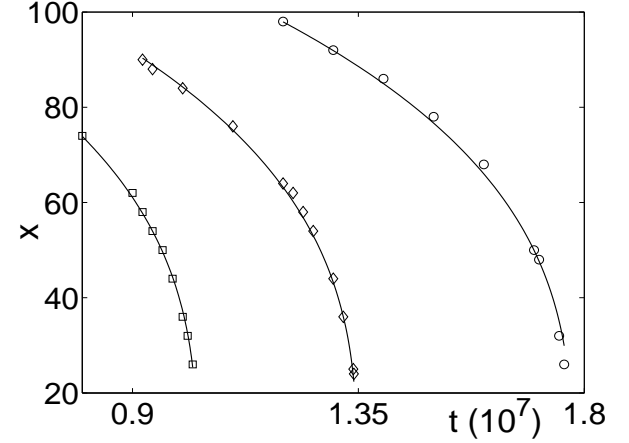


FIG. 20. Peak separation  $x$  as a function of time  $t$  for a two-mounded structure for model II with parallel updates (see text). The data shown are for  $\lambda=2.0, c=0.005, L=500$ . The initial value of the separation is  $x_0=80$  (squares),  $x_0=90$  (diamonds), and  $x_0=100$  (circles). The solid lines represent the fits described in the text.

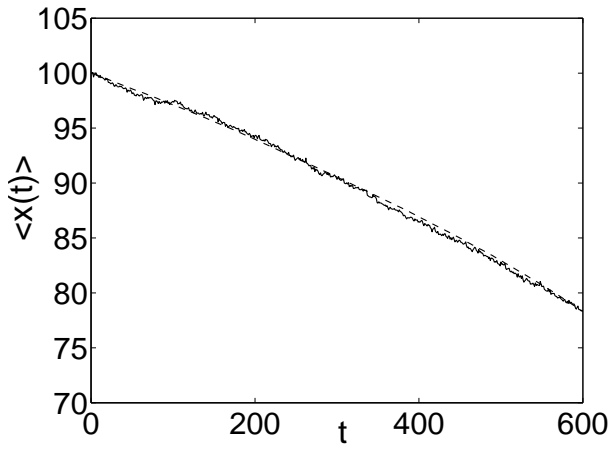


FIG. 21. The solid line shows the average value of the separation  $x(t)$  between mound tips (see text) as a function of time  $t$  for a two-mounded structure for model II. The data shown are for  $\lambda=2.0$ ,  $c=0.005$ ,  $L=500$ ,  $x_0=100$ , averaged over 800 runs. The dashed line shows  $\langle x(t) \rangle$  calculated for the reduced model of Eq.(21) with  $C = 285.0$  and  $D = 0.15$ .

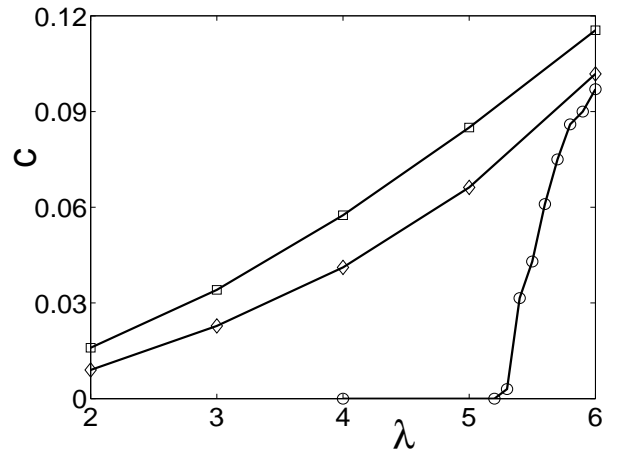


FIG. 23. Phase diagram for model I with conserved noise. The plots show 50% stability lines (see text) for a flat initial state (circles), an initial state with a pillar of height  $h_0 = 1000$  (diamonds) and an initial state identical to the mounded fixed point of the noiseless equations of motion (squares). The data were obtained from 100  $t = 10^4$  runs for  $L = 200$  samples.

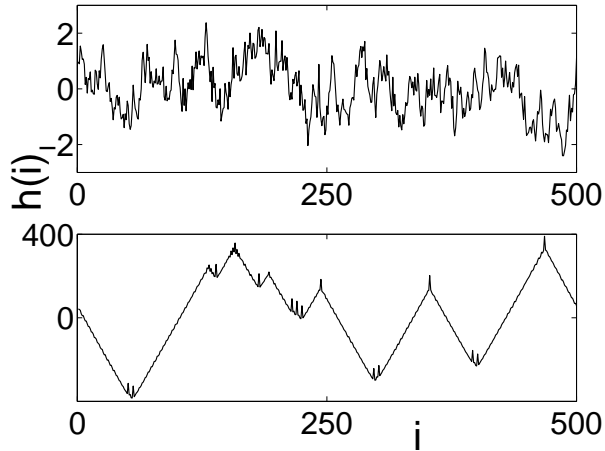


FIG. 22. Profiles at time  $t=10^5$  for model I with conserved noise ( $\lambda=4.0$ ,  $c=0.02$ ,  $L = 500$ ), for a flat initial configuration (top panel), and an initial configuration with a pillar of height  $h_0 = 1000$  (bottom panel).